

## Enteric neurons increase maternal food intake during reproduction

Dafni Hadjieconomou<sup>1,2</sup>, George King<sup>1,2</sup>, Pedro Gaspar<sup>1,2</sup>, Alessandro Mineo<sup>1,2</sup>, Laura Blackie<sup>1,2</sup>, Tomotsune Ameku<sup>1,2</sup>, Chris Studd<sup>1,2</sup>, Alex de Mendoza<sup>3,4</sup>, Fengqiu Diao<sup>5</sup>, Benjamin H. White<sup>5</sup>, Andre E. X. Brown<sup>1,2</sup>, Pierre-Yves Plaçais<sup>6</sup>, Thomas Prémat<sup>6</sup> and Irene Miguel-Aliaga<sup>1,2</sup>

<sup>1</sup> MRC London Institute of Medical Sciences, Imperial College London, Hammersmith Campus, Du Cane Road, London W12 0NN, UK

<sup>2</sup> Faculty of Medicine, Imperial College London, Hammersmith Campus, Du Cane Road, London W12 0NN, UK

<sup>3</sup> Australian Research Council Centre of Excellence in Plant Energy Biology, School of Molecular Sciences, The University of Western Australia, Perth, WA, 6009, Australia

<sup>4</sup> Harry Perkins Institute of Medical Research, Perth, WA, 6009, Australia

<sup>5</sup> Laboratory of Molecular Biology, National Institute of Mental Health, National Institutes of Health, Bethesda, United States

<sup>6</sup> Genes and Dynamics of Memory Systems, Brain Plasticity Unit, CNRS, ESPCI Paris, PSL Research University, 10 rue Vauquelin, 75005 Paris, France

**Females of many animal species increase their food intake during reproduction<sup>1-4</sup>, providing a physiologically relevant system to explore food intake regulation and its plasticity. Parsing enteric neuronal diversity in *Drosophila*, we identify a key role for gut-innervating neurons with sex- and reproductive state-specific activity in driving the maternal increase in food intake during reproduction. Steroid and gut enteroendocrine hormones functionally remodel these neurons, leading to post-mating release of their neuropeptide onto the muscles of the crop: a stomach-like organ. Post-mating neuropeptide release changes the dynamics of crop enlargement, leading to increased food intake. Preventing enteric neuron remodelling blunts reproductive hyperphagia and reduces reproductive fitness. Thus, plasticity of enteric neurons is key to reproductive success. Our findings may help explain why we “eat for two” during pregnancy, as well as the sex and reproductive biases of gastrointestinal conditions.**

The body's internal state has profound effects on brain functions; nutrient deficit or oestrous/reproductive state can shape sensory perception or central brain circuits with behavioural consequences<sup>5</sup>. Despite increasingly recognised roles for the gut-brain axis to maintaining energy balance<sup>6-11</sup>, links between internal state and gastrointestinal innervation remain poorly characterised. Progress has been hindered by its neuroanatomical complexity in mammalian systems, which is only beginning to be parsed<sup>6,12-16</sup>. The anatomically simpler –yet physiologically complex– *Drosophila* intestine provides an alternative entry point into the study of gastrointestinal innervation and its plasticity.

### **Innervation of the stomach-like crop**

Innervation of the main digestive portion of the adult fly intestine, encompassing the anterior midgut and the crop<sup>17,18</sup> (Extended Data Fig. 1a,b), emanates from an enteric (hypocerebral) ganglion (HCG) (Extended Data Fig. 1c,e,g,i,j) and central neurons of the brain's *pars intercerebralis* (PI) (Extended Data Fig. 1a,d,f,g). PI neurons directly innervate the anterior midgut and crop, and include insulin-producing neurons<sup>19-21</sup> and other peptidergic subtypes<sup>22</sup> (Extended Data Fig. 1a,d,f,g). The crop (but not the anterior midgut) is further populated by processes emanating from *corpora cardiaca* cells, which produce glucagon-like adipokinetic hormone (Akh) and are adjacent to the HCG (Extended Data Fig. 1h; Refs <sup>23,24</sup>). Adjacent to both the HCG and *corpora cardiaca* are the juvenile hormone-producing *corpus allatum* cells, which extend only short local projections (Extended Data Fig. 1c,k). The thoracico-abdominal ganglion of the central nervous system may not innervate these gut regions (Extended Data Fig. 1l,m).

The crop (an expandable structure commonly found in insect intestines<sup>18</sup>) might be disregarded as a passive food store, but several observations point to its active regulation. Refeeding flies following starvation resulted in enlarged, food-filled crops compared to those of flies fed *ad libitum*<sup>25</sup> (Extended Data Fig. 2a,d-e''), suggesting modulation of food ingestion into the crop. Live imaging or temporal dissections of flies fed dye-laced food revealed that food always enters the crop before proceeding to the midgut (Extended Data Fig. 2b-c'; Supplementary Video 1). Lastly, food transit through the crop is dependent on food palatability and its nutritional value (Extended Data Fig. 2f).

Thus, all food transits through the adult crop, which is nutrient-sensitive and shows chemically and anatomically diverse innervation.

### **Myosuppressin neuron control of the crop**

The crop and anterior midgut are innervated by Myosuppressin (Ms)-positive neurites<sup>26,27</sup>, which emanate from ~ 30 neurons located in the PI, and ~ 5 enteric neurons located in the HCG (Fig. 1a; Extended Data Fig. 3a,b,f,i-i'',o-o''). The PI Ms neurons are distinct from known PI neuronal subsets, with the exception of 8 Ms neurons that co-express the *Taotie-Gal4* marker (Extended Data Fig. 3l-n'',p-q''). Two PI populations of Ms-expressing neurons can be distinguished by size: ~ 18 large cells (including the *Taotie*-positive subset) and 12 smaller cells (Extended Data Fig. 3i-i''). Single-cell Flybow<sup>28</sup> clones revealed that the large Ms cells in the PI extend a single process that bifurcates into a longer axonal projection to the gut, which arborises in the HCG and extends further to innervate the crop, and a shorter, likely dendritic process that reaches the suboesophageal zone, where the axons of peripheral gustatory sensory neurons terminate (Extended Data Fig. 3c-e). A subset of HCG Ms-expressing neurons also innervates the crop, whereas another subset projects locally (Extended Data Fig. 3b and inset, respectively). We validated Ms expression using an endogenously tagged Ms reporter (Ms<sup>GFP</sup>, see Methods) and single molecule RNA *in situ* hybridisation (Extended Data Fig. 3j-k'). We also observed Ms-positive innervation of the hindgut, rectal ampulla and heart, and a subset of peripheral, sensory Ms-positive neurons innervating the female reproductive tract (Extended Data Fig. 3f-h; data not shown).

We used temporally controlled, adult-specific expression of TrpA1 and Kir2.1 to selectively activate or silence Ms neurons, respectively. Activation resulted in greatly enlarged crops in *ad libitum*-fed mated female flies, consistent with the relaxant properties of Ms on insect muscles *ex vivo*<sup>27,29</sup> (Fig. 1b-b''; Extended Data Fig. 4b,d-d''). By contrast, silencing of Ms neurons

prevented crop enlargement in a starved-refed situation in which the crop normally expands (Fig. 1c-c'', Extended Data Fig. 2a, 4c). Genetic downregulation or mutation of *Ms* (using a new mutant, see Methods) prevented crop enlargement, albeit to a lesser degree than *Ms* neuron silencing (Fig. 1d, Extended Data Fig. 4a-a'', e-e'', f-i). This could be due to another *Ms* neuron-derived neurotransmitter/neuropeptide contributing to crop enlargement, or to loss of *Ms* peptide during development in these experiments, resulting in adaptations rendering the crop more active than it would be in response to acute *Ms* peptide loss. We generated a *Gal4* insertion into the *Ms* locus that disrupts *Ms* production (*Ms*<sup>TGEM</sup>; see Methods). In contrast to the crop enlargement resulting from TrpA1-mediated activation from *Ms-Gal4*, TrpA1 expression from this (*Ms* mutant) *Ms*<sup>TGEM</sup>-*Gal4* driver failed to induce crop enlargement (Extended Data Fig. 4j,k), further confirming an *Ms* requirement.

We then sought to identify the *Ms* neuronal subset that controls crop enlargement. In contrast to downregulations in the HCG, *Ms* knockdown in the *Taotie-Gal4*-positive subset of large PI *Ms* neurons significantly reduced crop enlargement (Fig. 1d) (to a lesser degree than *Ms* neuron silencing, as expected from expression of *Taotie-Gal4* in only a subset of PI *Ms* neurons, Extended Data 3p-p''). TrpA1-driven activation of *Taotie-Gal4* neurons induced crop enlargement, even in the absence of food (Extended Data Fig. 4l,m). Thus, a subset of PI neurons induce and are indispensable for crop enlargement through their production of *Ms* neuropeptide.

We then explored contributions of Myosuppressin receptors 1 and 2 (*MsR1* and *MsR2*)<sup>30,31</sup> (Fig. 1e). Single-molecule RNA *in situ* hybridisation and a *MsR1 Gal4* reporter (*MsR1*<sup>TGEM</sup>, which is also an *MsR1* allele, see Methods) revealed *MsR1* expression in crop muscles, in subsets of neurons including enteric ganglia (HCG and *corpora cardiaca*) and neurons innervating the ovary and heart (although no *MsR1* expression was detected in ovarian/heart muscles) (Fig. 1f-g'; Extended Data Fig. 5a-h,j), consistent with transcriptomics data (Extended Data Fig. 5i). *MsR1*-positive neurons included the *Ms*-positive neurons of the PI and HCG (Extended Data Fig. 5f,g). Lower expression of *MsR2* was also detected in crop muscles (Fig. 1g'').

To investigate *Ms* receptor function, we downregulated *MsR1* specifically in adult crop muscles using two independent driver lines: *vm-Gal4* (expressed in all visceral muscles, leading to crop muscle-specific *MsR1* downregulation, given the neuron- and crop muscle-specific *MsR1* expression, Extended Data Fig. 5a-i), and *MsR1*<sup>CROP</sup>-*Gal4* (in which *MsR1-Gal4* neuronal expression is prevented using a pan-neuronal Gal80 driver). Both reduced crop enlargement in a starvation-refeeding assay, comparable to *Ms* silencing (Fig. 1h-h''; Extended Data Fig. 5k-o''). *MsR2* downregulation did not affect crop enlargement (Extended Data Fig. 5p). A role for *MsR1* in mediating crop enlargement was further confirmed using a *MsR1*<sup>TGEM</sup> mutant (see Methods; Extended Data Fig. 5q-s). Thus, *MsR1* is the crop muscle receptor through which *Ms* signals to modulate crop enlargement.

### Neuron remodelling during reproduction

We next explored the physiological regulation of crop enlargement, and found it to be dependent on sex and reproductive state; crops of *ad libitum*-fed mated females (used for all the experiments described above) were consistently more expanded than those of *ad libitum*-fed virgin female or mated male flies (Fig. 2a-a'',c). Since we failed to observe post-mating anatomical changes in *Ms* neuron projections (Extended Data Fig. 6a, b), we hypothesised that post-mating crop enlargement may result from preferential *Ms* release in mated females. *Ms*

transcript levels were unaffected by sex or reproductive status (Extended Data Fig. 6h), whereas Ms peptide in PI neuron cell bodies was lower in females only after mating (Fig. 2b-b'',d), consistent with a post-mating increase in Ms peptide secretion in females. This effect was specific to mating: nutrient availability failed to affect Ms levels in the PI Ms neuron cell bodies (Extended Data Fig. 6c-g). We also observed that more PI Ms neurons expressed a genetically encoded calcium-sensitive reporter (CaLexA, in which GFP expression is proportional to cumulative neuronal activity<sup>32</sup>) in mated females (Extended Data Fig. 6i-k). *In vivo* calcium imaging revealed that the Ms neurons of mated females had higher cumulative calcium levels and reduced calcium oscillations than those of virgin females (Fig. 2e-f'; Extended Data Fig. 6l). Physiologically, and in contrast to the effects seen in mated females, reducing Ms signalling in males or virgin female flies failed to impair crop enlargement. Indeed, when Ms signalling to crop muscles was prevented, the size of the crop of mated females was no longer significantly different from that of virgin females (Extended Data Fig. 6m,n). Collectively, these findings support the idea that, in females, mating changes the activity of PI Ms neurons to promote Ms release.

To establish how reproductive status is communicated to Ms neurons, we first focused on the steroid hormone ecdysone, which promotes egg production and is elevated post-mating<sup>33,34</sup>. The ecdysone receptor (EcR) is expressed by all PI Ms neurons (Extended Data Fig. 7a,a' and 8i), suggesting that they may be sensitive to circulating ecdysone. Adult- and Ms-neuron confined expression of a dominant-negative EcR receptor (which targets all EcR isoforms) or *EcR* downregulation (using RNAi lines that target all isoforms or the B1 isoform specifically; see Methods) reduced Ms levels to virgin-like levels in the Ms neuron cell bodies of mated females, whereas they had no effect in virgin females (Fig. 3a,a'; Extended Data Fig. 7b-d). They also increased the amplitude of *in vivo* calcium oscillations in Ms neuron cell bodies to virgin-like levels (Extended Data Fig. 8n,o). Compromising EcR signalling in the Ms neurons of adult females significantly reduced crop enlargement preferentially in mated females (Fig. 3b-b''; Extended Data Fig. 7e-j): a phenotype also apparent when the PI Ms neurons were targeted using *Taotie-Gal4* (Extended Data Fig. 9k,l). Hence, ecdysone communicates mating status to Ms neurons through its B1 receptor.

The adult intestine produces hormones that affect metabolism and fertility. We showed that mating resizes and metabolically remodels the adult intestine<sup>35</sup>, but did not investigate effects on its enteroendocrine cells. We now observe a post-mating increase in the total number of enteroendocrine cells, including a subset expressing Bursicon alpha hormone (Burs, recently shown to signal to adipose tissue via an unidentified neuronal relay<sup>36</sup>) (Fig. 3c-d; Extended Data Fig. 8a-c). An endogenous protein reporter for the Burs receptor Rickets (*Rk/Lgr2*)<sup>37</sup> revealed expression in subsets of neurons including all PI Ms neurons (including the *Taotie-Gal4*-positive subset) and projections terminating in the HCG (Extended Data Fig. 8d-j'; expression in a subset of the HCG Ms neurons was observed only sporadically, Extended Data Fig. 8e).

Consistent with regulation of Ms neurons by the post-mating increase in enteroendocrine Burs, adult-specific downregulation of the Burs receptor *rk* in Ms neurons reverted Ms levels to virgin-like levels in the Ms neuron cell bodies of mated females, whereas it had no effect in virgin females (Fig. 3e-e''; Extended Data Fig. 8k-m). Like *EcR* downregulation, *rk* downregulation in Ms neurons also increased the amplitude of *in vivo* calcium oscillations in the Ms neuron cell bodies of mated females to virgin-like levels (Extended Data Fig. 8n,o). Functionally, both adult-specific downregulation of *rk* in Ms neurons and *Burs* downregulation from intestinal

enteroendocrine cells preferentially reduced crop enlargement in mated females (Fig. 3f-f''; Extended Data Fig. 9a-e). Adult-specific *rk* downregulation from *Taotie-Gal4* also reduced crop enlargement in mated females, confirming a contribution of the *rk*- and *Taotie-Gal4*-positive subset of PI Ms neurons (Extended Data Fig. 9k,l). By contrast, stimulating intestinal release of enteroendocrine hormones including Burs from enteroendocrine cells resulted in reduced, mated-like Ms levels in the Ms neuron cell bodies of virgin females (Extended Data Fig. 9f-h), and greatly enlarged crops (Extended Data Fig. 9i-j,i) (see also Extended Data Fig. 8a'-a''' for co-expression of *Tkg-Gal4* enteroendocrine cell driver and Burs).

Thus, a steroid and a gut enteroendocrine hormone communicate mating status to the brain. Acting through their receptors in the PI Ms neurons, these hormones change Ms neuronal activity, promoting Ms release after mating (Extended Data Fig. 9m).

### Neuron remodelling promotes food intake

To investigate the physiological significance of post-mating Ms neuron modulation, we selectively prevented crop enlargement post-mating by downregulating *MsR1* specifically in adult crop muscles using two independent strategies (Extended Data Fig. 5k,l). This did not affect physiological features of males or virgin females (including food intake), but did prevent the increase in food intake observed in female flies after mating<sup>1</sup> (Fig. 4a,b; Extended Data Fig. 10a-e). Comparable results were obtained by blocking the post-mating ecdysone and Burs inputs into the Ms neurons (Fig. 4c,d; Extended Data Fig. 10f,g). *MsR2* downregulation had no such effect (Extended Data Fig. 10d). Thus, the post-mating change in crop expandability mediated by Ms/*MsR1* signalling is causal to the increased food intake observed in females after mating.

The negative pressures reported in the crop of larger insects<sup>38</sup> suggest that the crop may draw food in by generating suction. The increased crop expandability enabled by post-mating Ms release could therefore increase food intake through changes in suction. We observed that mated females ingest more food per sip than virgin females (Supplementary Table 1), consistent with mated females needing to generate a higher suction pressure to facilitate bigger sips. We therefore modelled crop enlargement by using the Poiseuille equation for incompressible fluid flow in a pipe (see Methods), and found that the crop would need a suction pressure on the order of -1kPa to achieve the intake volume previously reported per sip<sup>39</sup>. This is in reasonable agreement with previously reported values measured in cockroach crops of between -0.5 and -1kPa<sup>38</sup>. The model predicts that mated flies would require a modest increase in suction pressure to -1.3kPa to facilitate the increased sip size.

In the model, crop volume drives food intake via increased suction (Extended Data Fig. 10h). Hence, a crop that cannot enlarge or a persistently enlarged crop should both result in a comparable reduction in food intake by preventing suction generation. We tested this by constitutively preventing crop enlargement (using crop muscle-specific *MsR1* knockdown, Extended Data Fig. 5k,l), or by constitutively inducing it (using TrpA1-mediated Ms neuron activation from *Ms-Gal4* or *Taotie-Gal4*, Extended Data Fig. 4l,m), after which we assessed food intake by switching flies from undyed to dye-laced food. Both genetic manipulations indeed reduced intake of the dye-laced food (Extended Data Fig. 10c-e,i,j,m). Conversely, increasing the rate at which the crop expands should increase food intake. We tested this by genetically activating the Ms neurons as in the previous experiment, but this time we switched the flies to dye-laced food and monitored their intake at the same time as we activated the neurons (i.e. as we were inducing greater crop expansion) rather than after a persistent activation (when the

crop is already maximally expanded). We observed increased food intake in these conditions (Extended Data Fig. 10k,l,n). Although further work will be required to elucidate the full dynamics of crop enlargement, filling and emptying, these experiments support the idea that the Ms-induced post-mating enlargement of the crop increases food intake at least partly through increasing the crop's suction power.

Finally, given the links between nutrient intake and fecundity<sup>40</sup>, we hypothesised that the Ms-driven post-mating crop enlargement may be adaptive and support reproduction. We tested this; selectively preventing crop enlargement post-mating by downregulating *MsR1* as previously significantly reduced egg production (Fig. 4e; Extended Data Fig. 10o). Eggs that were produced also showed reduced viability (Extended Data Fig. 10p). Thus, the crop and its Ms innervation help sustain the post-mating increase in food intake, maximising female fecundity.

## DISCUSSION

We reveal an unexpected role for the crop (a stomach-like organ) in maximising reproductive output. Preventing its Ms-mediated post-mating enlargement blunts the post-mating increase in food intake and reduces egg production, suggesting an adaptive role for hyperphagia during reproduction. We propose that the crop is a key reproductive organ, and Ms a major effector of post-mating responses. In support of this idea, the crop is only present in adults. The contributions of the crop to reproduction may extend beyond reproductive hyperphagia; certain Diptera species have co-opted the crop for reproduction-related behaviours such as regurgitation of nuptial gifts or secretion of male pheromones<sup>18</sup>. Finally, Ms receptors are closely related to Sex peptide receptor (the “mating sensor” of female flies), and both co-evolved following duplication of an ancestral receptor which might have responded to the Myoinhibitory peptide (Mip) in the last common ancestor of protostomes<sup>41</sup> (Fig. 1e). We are finding that other post-mating features of female physiology<sup>20</sup> are also affected when we interfere with Ms signalling more broadly. It will be interesting to explore possible links between Ms and Sex peptide signalling.

We provide evidence for a gut-to-brain axis in flies by identifying central Ms neurons as a target of an enteroendocrine hormone. These central neurons innervate the gut, “closing” a gut-brain-gut loop that connects a midgut hormone to the crop, a more anterior gut region. Such a loop may coordinate functions of different intestinal portions, whilst enabling its central modulation by sensory cues (e.g. gustatory). We also identify the Ms neurons as the neural targets of ecdysone which had been shown to promote food intake<sup>42</sup>. In light of increasing evidence for significant and lasting effects of reproduction on the human female brain<sup>43,44</sup>, Ms neurons provide a tractable and physiological significant neural substrate to investigate the neuronal modulation of feeding by sex and reproductive state.

Finally, our own digestive system may be similarly modulated by reproductive cues to affect food intake. Enteric neurons express sex/reproductive hormone receptors<sup>45</sup> and reproductive changes in enteroendocrine peptide levels have been reported<sup>3</sup>. We argue that pregnancy and lactation represent an attractive, relatively unexplored physiological adaptation to investigate nutrient intake regulation, organ remodelling and metabolic plasticity, which might eventually provide new ways to curb appetite and/or weight gain.

- 1 Carvalho, G. B., Kapahi, P., Anderson, D. J. & Benzer, S. Allocrine modulation of feeding behavior by the Sex Peptide of *Drosophila*. *Curr Biol* **16**, 692-696, doi:10.1016/j.cub.2006.02.064 (2006).
- 2 Gittleman, J. L. & Thompson, S. D. Energy Allocation in Mammalian Reproduction. *Amer Zool* **28**, 863-875 (1988).
- 3 Johnson, M. L., Saffrey, M. J. & Taylor, V. J. Gastrointestinal capacity, gut hormones and appetite change during rat pregnancy and lactation. *Reproduction*, doi:10.1530/REP-18-0414 (2019).
- 4 Speakman, J. R. The physiological costs of reproduction in small mammals. *Philos Trans R Soc Lond B Biol Sci* **363**, 375-398, doi:10.1098/rstb.2007.2145 (2008).
- 5 Grunwald Kadow, I. C. State-dependent plasticity of innate behavior in fruit flies. *Curr Opin Neurobiol* **54**, 60-65, doi:10.1016/j.conb.2018.08.014 (2019).
- 6 Bai, L. *et al.* Genetic Identification of Vagal Sensory Neurons That Control Feeding. *Cell* **179**, 1129-1143 e1123, doi:10.1016/j.cell.2019.10.031 (2019).
- 7 Han, W. *et al.* A Neural Circuit for Gut-Induced Reward. *Cell* **175**, 887-888, doi:10.1016/j.cell.2018.10.018 (2018).
- 8 Soty, M., Gautier-Stein, A., Rajas, F. & Mithieux, G. Gut-Brain Glucose Signaling in Energy Homeostasis. *Cell Metab* **25**, 1231-1242, doi:10.1016/j.cmet.2017.04.032 (2017).
- 9 Talbot, J. *et al.* Feeding-dependent VIP neuron-ILC3 circuit regulates the intestinal barrier. *Nature*, doi:10.1038/s41586-020-2039-9 (2020).
- 10 Tan, H.-E. *et al.* The gut–brain axis mediates sugar preference. *Nature* **580**, 511–516 (2020).
- 11 Zimmerman, C. A. *et al.* A gut-to-brain signal of fluid osmolarity controls thirst satiation. *Nature* **568**, 98-102, doi:10.1038/s41586-019-1066-x (2019).
- 12 Drokhyansky, E. *et al.* The enteric nervous system of the human and mouse colon at a single-cell resolution. *bioRxiv*, doi:<https://doi.org/10.1101/746743> (2019).
- 13 Kaelberer, M. M. *et al.* A gut-brain neural circuit for nutrient sensory transduction. *Science* **361**, doi:10.1126/science.aat5236 (2018).
- 14 Lasrado, R. *et al.* Lineage-dependent spatial and functional organization of the mammalian enteric nervous system. *Science* **356**, 722-726, doi:10.1126/science.aam7511 (2017).
- 15 Williams, E. K. *et al.* Sensory Neurons that Detect Stretch and Nutrients in the Digestive System. *Cell* **166**, 209-221, doi:10.1016/j.cell.2016.05.011 (2016).
- 16 Zeisel, A. *et al.* Molecular Architecture of the Mouse Nervous System. *Cell* **174**, 999-1014 e1022, doi:10.1016/j.cell.2018.06.021 (2018).
- 17 Miguel-Aliaga, I., Jasper, H. & Lemaitre, B. Anatomy and Physiology of the Digestive Tract of *Drosophila melanogaster*. *Genetics* **210**, 357-396, doi:10.1534/genetics.118.300224 (2018).
- 18 Stoffolano, J. G., Jr. & Haselton, A. T. The adult Dipteran crop: a unique and overlooked organ. *Annu Rev Entomol* **58**, 205-225, doi:10.1146/annurev-ento-120811-153653 (2013).
- 19 Cao, C. & Brown, M. R. Localization of an insulin-like peptide in brains of two flies. *Cell Tissue Res* **304**, 317-321 (2001).
- 20 Cognigni, P., Bailey, A. P. & Miguel-Aliaga, I. Enteric neurons and systemic signals couple nutritional and reproductive status with intestinal homeostasis. *Cell Metab* **13**, 92-104, doi:10.1016/j.cmet.2010.12.010 (2011).
- 21 Rulifson, E. J., Kim, S. K. & Nusse, R. Ablation of insulin-producing neurons in flies: growth and diabetic phenotypes. *Science* **296**, 1118-1120, doi:10.1126/science.1070058 (2002).

- 22 Dus, M. *et al.* Nutrient Sensor in the Brain Directs the Action of the Brain-Gut Axis in Drosophila. *Neuron* **87**, 139-151, doi:10.1016/j.neuron.2015.05.032 (2015).
- 23 Kim, S. K. & Rulifson, E. J. Conserved mechanisms of glucose sensing and regulation by Drosophila corpora cardiaca cells. *Nature* **431**, 316-320, doi:10.1038/nature02897 (2004).
- 24 Lee, G. & Park, J. H. Hemolymph sugar homeostasis and starvation-induced hyperactivity affected by genetic manipulations of the adipokinetic hormone-encoding gene in Drosophila melanogaster. *Genetics* **167**, 311-323 (2004).
- 25 Edgecomb, R. S., Harth, C. E. & Schneiderman, A. M. Regulation of feeding behavior in adult Drosophila melanogaster varies with feeding regime and nutritional state. *J Exp Biol* **197**, 215-235 (1994).
- 26 McCormick, J. & Nichols, R. Spatial and temporal expression identify dromyosuppressin as a brain-gut peptide in Drosophila melanogaster. *J Comp Neurol* **338**, 278-288 (1993).
- 27 Richer, S., Stoffolano, J. G., Jr., Yin, C. M. & Nichols, R. Innervation of dromyosuppressin (DMS) immunoreactive processes and effect of DMS and benzethonium chloride on the *Phormia regina* (Meigen) crop. *J Comp Neurol* **421**, 136-142 (2000).
- 28 Hadjieconomou, D. *et al.* Flybow: genetic multicolor cell labeling for neural circuit analysis in Drosophila melanogaster. *Nat Methods* **8**, 260-266, doi:10.1038/nmeth.1567 (2011).
- 29 Holman, G. M., Cook, B. J. & Nachman, R. J. Isolation, primary structure and synthesis of leucomyosuppressin, an insect neuropeptide that inhibits spontaneous contractions of the cockroach hindgut. *Comparative Biochemistry and Physiology Part C: Comparative Pharmacology* **85**, 329-333 (1986).
- 30 Egerod, K. *et al.* Molecular cloning and functional expression of the first two specific insect myosuppressin receptors. *Proc Natl Acad Sci U S A* **100**, 9808-9813, doi:10.1073/pnas.1632197100 (2003).
- 31 Leander, M. *et al.* Cardiac contractility structure-activity relationship and ligand-receptor interactions; the discovery of unique and novel molecular switches in myosuppressin signaling. *PLoS One* **10**, e0120492, doi:10.1371/journal.pone.0120492 (2015).
- 32 Masuyama, K., Zhang, Y., Rao, Y. & Wang, J. W. Mapping neural circuits with activity-dependent nuclear import of a transcription factor. *J Neurogenet* **26**, 89-102, doi:10.3109/01677063.2011.642910 (2012).
- 33 Harshman, L. G., Loeb, A. M. & Johnson, B. A. Ecdysteroid titers in mated and unmated Drosophila melanogaster females. *J Insect Physiol* **45**, 571-577 (1999).
- 34 Schwedes, C. C. & Carney, G. E. Ecdysone signaling in adult Drosophila melanogaster. *J Insect Physiol* **58**, 293-302, doi:10.1016/j.jinsphys.2012.01.013 (2012).
- 35 Reiff, T. *et al.* Endocrine remodelling of the adult intestine sustains reproduction in Drosophila. *Elife* **4**, e06930, doi:10.7554/eLife.06930 (2015).
- 36 Scopelliti, A. *et al.* A Neuronal Relay Mediates a Nutrient Responsive Gut/Fat Body Axis Regulating Energy Homeostasis in Adult Drosophila. *Cell Metab* **29**, 269-284 e210, doi:10.1016/j.cmet.2018.09.021 (2019).
- 37 Diao, F., Elliott, A. D., Diao, F., Shah, S. & White, B. H. Neuromodulatory connectivity defines the structure of a behavioral neural network. *Elife* **6**, doi:10.7554/eLife.29797 (2017).
- 38 Davey, K. G. & Trehere, J. E. Studies on Crop Function in the Cockroach (*Periplaneta Americana* L.). *J Exp Biol* **41**, 513-524 (1964).
- 39 Itskov, P. M. *et al.* Automated monitoring and quantitative analysis of feeding behaviour in Drosophila. *Nat Commun* **5**, 4560, doi:10.1038/ncomms5560 (2014).

- 40 Chapman, T. & Partridge, L. Female fitness in *Drosophila melanogaster*: an interaction between the effect of nutrition and of encounter rate with males. *Proc Biol Sci* **263**, 755-759, doi:10.1098/rspb.1996.0113 (1996).
- 41 Poels, J. *et al.* Myoinhibiting peptides are the ancestral ligands of the promiscuous *Drosophila* sex peptide receptor. *Cell Mol Life Sci* **67**, 3511-3522, doi:10.1007/s00018-010-0393-8 (2010).
- 42 Sieber, M. H. & Spradling, A. C. Steroid Signaling Establishes a Female Metabolic State and Regulates SREBP to Control Oocyte Lipid Accumulation. *Curr Biol* **25**, 993-1004, doi:10.1016/j.cub.2015.02.019 (2015).
- 43 Brunton, P. J. & Russell, J. A. The expectant brain: adapting for motherhood. *Nat Rev Neurosci* **9**, 11-25, doi:10.1038/nrn2280 (2008).
- 44 Hoekzema, E. *et al.* Pregnancy leads to long-lasting changes in human brain structure. *Nat Neurosci* **20**, 287-296, doi:10.1038/nn.4458 (2017).
- 45 Ameku, T., Beckwith, H., Blackie, L. & Miguel-Aliaga, I. Food, microbes, sex and old age: on the plasticity of gastrointestinal innervation. *Curr Opin Neurobiol* **62**, 83-91, doi:10.1016/j.conb.2019.12.004 (2020).

### Fig. 1. *Ms*/*MsR1* expression and their regulation of crop enlargement

**a**, *Ms*-*Gal4*-driven EGFP expression in the adult fly brain-gut axis (in green). Gut muscles are labelled in blue with phalloidin. **b-c**, Crop phenotypes resulting from *Ms*-*Gal4*-driven *Ms* neuron activation/silencing. **b-b''**, Activation (*TrpA1* expression, 4h at the permissive temperature) leads to enlarged crops (**b**) compared to heterozygous genetic controls (**b',b'**) in *ad libitum*-fed flies. **c-c''**, Silencing (*Kir2.1* expression-temporally confined with *tub-Gal80<sup>TS</sup>*) leads to smaller crops (**c**) compared to their heterozygous genetic controls in starved-refed flies (**c,c''**). **d**, *Ms* knockdown in different *Ms*-producing neuronal subtypes. *Ms-Gal4*, *Mip-Gal4* or *Taotie-Gal4*-driven downregulation of *Ms* expression from all, HCG or PI *Ms*-expressing neurons, respectively. Similar to *Ms-Gal4*, *Taotie-Gal4*-driven, but not *Mip-Gal4*-driven downregulation significantly reduced crop area. **e**, Phylogenetic analysis of Myosuppressin receptors. **f**, *MsR1* expression in crop muscles (driven by the endogenous protein reporter *MsR1<sup>TGEM</sup>-Gal4*). Expression is apparent in crop muscles (labelled in blue with phalloidin) and along the crop nerves. **g-g''**, RNA FISH of *MsR1* and *MsR2* mRNAs in crop muscles; *MsR1* (in green) is more readily detected than *MsR2* (in red). Muscle cell nuclei are shown in blue by DAPI staining. **g'** and **g''** show single FISH channels for clarity. **h-h''**, Crops of starved-refed flies following downregulation of *MsR1* in visceral muscles. Crop size is reduced upon *MsR1* downregulation (**h**), compared to *UAS* (**h'**) and *Gal4* (**h''**) controls. Scale bars: **a, f** = 50µm, **g-g''**=10µm and **b-c''** and **h-h'** = 500µm. Sample sizes: **a, f** =10-25, **b-b''**=10-15, **c-c''**=26-31, **d**=10-28, **g-g''**=10-15, **h-h''**=22-24. See Supplementary Information for a list of full genotypes. Statistics: Kruskal Wallis test. Boxplots: all data points shown, line, median, whiskers min and max. p>0.05; \*: 0.05>p>0.01; \*\*: 0.01>p>0.001; \*\*\*: p<0.001.

### Fig. 2. Reproductive modulation of *Ms* neurons

**a-b''**, Dissected intestines (top) or *Ms* stainings (bottom) of *ad libitum*-fed wild-type flies. Mated females have more enlarged crops (**a''**) and less *Ms* in their cell bodies (**b''**) than virgin females (**a',b'**) or mated males (**a,b**). In **b-b''**, fluorescence signals are pseudo-coloured; high to low intensity is displayed as warm (yellow) to cold (blue) colours here and thereafter. **c**, Quantifications of crop area in *ad libitum*-fed wild-type mated females, virgin females or males. The crops of mated females are larger. **d**, Quantification of *Ms* staining in mated male, virgin female and mated female brains. Each point corresponds to a separate image. Less peptide is detected in virgin females and, especially, mated females when compared to males. **e**, Quantification of the amplitude of GCaMP fluorescence oscillations in *Ms* neurons of virgin females and mated females. Each data point corresponds to an individual cell measurement.

Reduced amplitude is detected in mated females. In **c-e**, grey box: mated male, pink box: virgin female, red box: mated female. **f,f'**, *In vivo* calcium brain imaging of Ms neurons using the GCaMP6 sensor. Temporally defined video snapshots of Ms-driven GCaMP6 activity in the PI of virgin (**f**), or mated (**f'**) females, imaged over 1000 frames (frs, each frame acquired every 427 milliseconds). Asterisks and arrows highlight two randomly chosen Ms neurons so that their calcium signal can be readily followed across snapshots. Scale bars = 20µm except for **a-a''** = 500µm. Sample sizes: **a-a''** and **c** =6-9, **b-b''** and **d** =14-26 and **e-f''** =19-25. See Supplementary Information for a list of full genotypes. Statistics: **c-d**, Kruskal Wallis and **e**, Mann-Whitney-Wilcoxon test. Boxplots: all data points shown, line, median, whiskers min and max.  $p>0.05$ ; \*:  $0.05>p>0.01$ ; \*\*:  $0.01>p>0.001$ ; \*\*\*:  $p<0.001$ .

**Fig. 3. Steroid and enteroendocrine hormones remodel Ms neurons to increase crop expandability**

**a-b''**, Representative Ms peptide levels (**a-a''**) or crops following starvation-refeeding (**b-b''**) in mated females following adult-specific, *Ms-Gal4*-driven expression of *EcR<sup>DN</sup>*. Higher Ms levels in the PI Ms neuron cell bodies (**a**) and smaller crops (**b**) are apparent relative to *UAS* (**a',b'**) and *Gal4* (**a'',b''**) controls. Fluorescence signals are pseudo-coloured; high to low intensity is displayed as warm (yellow) to cold (blue) colours. **c'-c'''**, Expression of the enteroendocrine marker Prospero (Pros, in white) and the enteroendocrine hormone Burs (in red) in midguts of virgin (**c,c'**), and mated (**c'',c'''**) female flies, showing increased Burs expression and enteroendocrine cell number in mated female flies. Filled arrow heads point to Pros and Burs-positive cells, empty arrowheads point to Pros-positive/Burs-negative cells. Images in red, full z projections; images in white below them, single z slices. **d**, Quantification of Burs-expressing enteroendocrine cells (assessed as the number of Pros- and Burs-positive cells), revealed higher numbers in mated females compared to virgins. **e-f''**, Representative Ms peptide levels (**e-e''**) or crops following starvation-refeeding (**f-f''**) in mated females following adult-specific, *Ms-Gal4*-driven *rk* downregulation. Higher Ms levels in the PI Ms neuron cell bodies (**e**) and smaller crops (**f**) are apparent relative to *UAS* (**e',f'**) and *Gal4* (**e'',f''**) controls. Scale bars: **a-a''**, **e-e''** = 20µm, **c-c'** = 50µm and **b-b''**, **f-f''** = 500µm. Sample sizes: **a-a''** = 26-29, **b-b''** = 20-24, **c-c'''** = 10-15, **d** = 5 (midguts counted), **e-e''** = 14-19, **f-f''** = **n** = 3 (imaged, 3-39 quantified). See Supplementary Information for a list of full genotypes. Statistics: Mann-Whitney-Wilcoxon test. Boxplots: all data points shown, line, median, whiskers min and max.  $p>0.05$ ; \*:  $0.05>p>0.01$ ; \*\*:  $0.01>p>0.001$ ; \*\*\*:  $p<0.001$ .

**Fig. 4. Post-mating, Ms-mediated crop enlargement increases food intake and reproductive output**

**a-b**, Effect of adult-specific downregulation of *MsR1* in visceral muscles on feeding. Reduced amount of dye-laced food ingested during the course of 20min (**a**) and mean number of sips per fly over 1h of feeding (**b**) are apparent following downregulation relative to *Gal4* and *UAS* controls. **c-d**, Quantifications of ingested dye-laced food following downregulation of *EcR* in Ms neurons (**c**) or *Burs* in Pros-expressing enteroendocrine cells (**d**) of starved-refed mated females. Both result in reduced food intake relative to *Gal4* and *UAS* controls. **e**, Reduced Ms signalling to crop muscles reduces fecundity. Data are provided as numbers or eggs laid by mated females per day over the course of 4 days. *MsR1* expression in crop muscles (*vm<sup>TS</sup> > MsR1-RNAi*) is shown in red and the two genetic controls are shown in grey. Sample sizes: **a** = 17-20, **b** = 34-40, **c** = 24-57, **d** = 39-90, **e** = 120. See Supplementary Information for a list of full genotypes. Statistics: **a-d**, Kruskal Wallis and **e**, two-way ANOVA followed by a Tukey's multiple comparison test, day and genotype were the 2 independent factors. Boxplots: all data points shown, line, median, whiskers min and max.  $p>0.05$ ; \*:  $0.05>p>0.01$ ; \*\*:  $0.01>p>0.001$ ; \*\*\*:  $p<0.001$ .

## Methods

### Fly husbandry

Fly stocks were reared on a standard cornmeal/agar diet (6.65% cornmeal, 7.1% dextrose, 5% yeast, 0.66% agar supplemented with 2.2% nipagin and 3.4% propionic acid). All experimental flies were kept in incubators at 65% humidity and on a 12h light/dark cycle, at 18°C, 25°C or 29°C depending on the specific experiment. Flies were transferred to fresh vials every 3 days, and fly density was kept to a maximum of 20 flies per vial. 4-day and 7-day-old virgin flies were used for experiments at 18°C and 25°C respectively unless otherwise indicated.

### Temperature-controlled experiments

We used *UAS-TrpA1* to activate Ms neurons (neuropeptide release) and to force release of peptides (including Burs) from enteroendocrine cells. For activation of Ms neurons to assess crop enlargement/feeding, we transferred flies to a 29°C incubator for 4h prior to transfer to dye-laced food, or for 1h acute activation experiments (to allow crop expansion during feeding before it reaches maximum size, Extended Data Fig. 10k,l,n). In starved-refed scenarios, feeding was monitored over the course of 15-20min, whereas in fed *ad libitum* conditions feeding was monitored over the course of 2h (or 1h when comparing pre-activation with concurrent activation of Ms neurons with feeding). To force enteroendocrine peptide release we extended the incubation at 29°C to 14-16h. For Ms neuron silencing (neuropeptide retention) we used the ubiquitously expressed temperature sensitive Gal80 allele (*tub-Gal80<sup>TS</sup>*) recombined with the *UAS-kir2.1* transgene. Flies were reared, aged and mated at 18°C. They were then transferred for 24h at 29°C and either starved or kept feeding *ad libitum* for an additional 14-16h at 29°C. Next, experimental assays were carried out at 29°C.

RNAi experiments were also performed at 29°C unless otherwise indicated. For these, flies were reared and aged at permissive temperature (18°C) and then transferred at 29°C for RNAi induction for 5 days. Experimental assays were carried out at 29°C.

*Ms-Gal4* Flybow clones were generated using the Flybow 1.1 construct based on the method described in<sup>28</sup>. A multiple heat-shock approach at different developmental timepoints was used. Each heat-shock lasted 1h at 37°C.

### Diets

For the experiments exploring the dietary regulation of crop enlargement, we used agar-based diets with a single nutrient source supplemented with 1% E133 Duracolor brilliant blue FCF (referred to as FCF blue). The basic recipe contained 1% agar, 1% FCF blue, 2.2% nipagin and 3.4% propionic acid. Each specific nutrient was added to the basic recipe in the following amounts: sorbitol only 18.216% (1M), yeast only 5%, arabinose only 15.012% (1M) and sucrose only 34.230% (1M). For details of the used of these diets and their palatability/nutritional value see<sup>46-48</sup>. Times displayed in Extended Data Fig. 2b-b''' panels correspond to times after initiation of feeding of the dye-laced diets; only flies that continued to engage with the food following initiation of feeding were dissected and scored.

To assess the effect of starvation on Ms levels, 4-5 day-old virgin female flies or female flies mated for 24h were starved in 1% agar for 16h prior to immunohistochemical analysis.

For fecundity assays, which required daily egg counting, experimental flies were kept in cages on apple juice plates with a smear of live yeast. Plates were changed every 24h.

Refeeding assays required visualization and/or quantitation of food in the fly gut. For these, 1% FCF blue was added to the standard fly food. When pre-starvation was required, flies were kept in vials containing 1% agar in Milli-Q water, with 2.2% nipagin and 0.34% propionic acid.

flyPAD food was pan-cooked using 1% agarose, 5% live yeast (*S. cerevisiae*) and 7.1% dextrose. It was dispensed into 2mL Eppendorf tubes and stored at -20°C until used. The food was melted to liquid form using a heat-block at 95°C. It was then dispensed as a viscous droplet in the flyPAD set up, where it fully solidified.

### Fly stocks

Drivers: *nSyb-Gal4* (original insert on 3<sup>rd</sup> chromosome, gift from Julie Simpson), *Ilp2-3-Gal4*<sup>49</sup>, *Gr43a<sup>KI</sup>-Gal4*<sup>50</sup>, *Dh44-Gal4*<sup>51</sup>, *Mip-Gal4*<sup>52</sup>, *pain-Gal4*<sup>53</sup>, *Gr28a-Gal4*<sup>54</sup>, *Aug21-Gal4* (BDSC: 30137), *Ubx-Gal4*<sup>55</sup>, *abd-A-Gal4*<sup>56</sup>, *Ms-Gal4*<sup>57</sup>, *Taotie-Gal4*<sup>58</sup>, *Dsk-Gal4*<sup>57</sup>, *MsR1<sup>TGEM</sup>-Gal4* (this study), *vm-Gal4*<sup>59</sup>, *rk<sup>TGEM</sup>-Gal4*<sup>37</sup>, *voila-Gal4* (<sup>60</sup>, stock combined with *tub-Gal80<sup>TS</sup>* was a gift from Julia Cordero), *Tkg-Gal4*<sup>61</sup>, *tub-Gal80<sup>TS62</sup>*, *nsyb-Gal80* (<sup>63</sup>, gift from Julie Simpson).

Reporters: *Ms<sup>GFP</sup>* (this study), *UAS-FB1.1* (ref. <sup>28</sup>), *UAS-DenMark-RFP*, *UAS-Venus-pm* (<sup>64,65</sup>, recombinant was a gift from Matthias Landgraf), *UAS-hs-mFlp5* (ref. <sup>28</sup>), *UAS-TrpA1* (ref. <sup>66</sup>), *UAS-Kir2.1* (ref. <sup>67</sup>), *UAS-Ms-RNAi* (VDRC: GD 4874), *UAS-Ms-RNAi* (TRiP: JF02144), *UAS-stingerGFP* (ref. <sup>68</sup>), *UAS-MsR1-RNAi* (VDRC: GD 9369), *UAS-MsR2-RNAi* (VDRC: GD 42304), *UAS-CaLexA* (ref. <sup>32</sup>), *UAS-GCaMP6f* ref. <sup>69</sup>), *UAS-EcR-RNAi*<sup>97</sup> (BDSC: 9326, referred to as *EcR<sup>RNAi-1</sup>*), *UAS-EcR.B1-RNAi*<sup>168</sup> (BDSC: 9329, referred to as *EcR<sup>RNAi-2</sup>*), *UAS-EcR-RNAi* (VDRC: GD 37058, referred to as *EcR<sup>RNAi-3</sup>*), *UAS-EcR<sup>DN</sup>* (BDSC: 6872), *UAS-rk-RNAi* (VDRC: GD 29932), *UAS-dcr2* (VDRC: 60010), *UAS-Burs-RNAi* (VDRC: GD 3951).

Mutants: *MS<sup>Δ</sup>* (this study), *Df(3R)Exel6199* (BL7678), *MsR1<sup>TGEM</sup>-Gal4* (this study), *Ms<sup>TGEM</sup>-Gal4* (this study), *Df(3L)Aprt-32* (BDSC: 5411).

*Oregon R* (*OrR*) and *w<sup>1118</sup>* were used as control flies

Generation of *Ms<sup>GFP</sup>* transgenic reporter line. The CBGtg9060F04101D GFP-tagged clone for *Ms* from the fosmid library TransgeneOme Resource (Source Bioscience<sup>70</sup>) was used to establish transgenic lines using  $\phi$ C-31 integrase mediated recombination (BestGene). The landing *attP* site used was *att40(y<sup>1</sup> w<sup>67c23</sup>; P{CaryP}attP40)*.

### Generation of *Ms<sup>Δ</sup>* null mutant

*Ms<sup>Δ</sup>* was generated using CRISPR/cas9 assisted homologous recombination as described in<sup>71</sup>. The entire coding region of the gene was removed and replaced with an *attP* site and an excisable Pax3-mCherry cassette. We chose to use a two-gRNA approach (gRNA1: 5'-TTTTAGAGCTAGAAATAG-3' and gRNA2: 5'-AACACCACTTGGTCCCGA-3'), making use of the *pCFD4* vector (Addgene #49411). The two homology arms were cloned in the modified *pTV3-mCherry* vector (gift from Cyrille Alexandre). Both vectors were injected into *yw; nos Cas9(II-attP40)* flies by BestGene.

5'-Homology arm:

```
GTGCTTGCCTTCAACAAGTCCAGCAAACAGAGCAGCAGCTGAACCCCGGTGTTAACAACCTAACAAGTTT
GTCCATTAACCTCTTTGTGGAAGCACCGATACCTCAAAGCCCTCATCAGGTGGGTACTTGTGTCTTGAG
ATGTGCAGAGTGATAGATACTTTAGAGGAATAACTGAATACATATAAAGTGAATCCTTGAGGTTTCAGT
CGAAAGGTGTGAAAGATAAAGCCTGTATTAAGTGTGTACATTTGTGAAAATATGGTACTATCATAAT
GATGGCTTTATACTTAATTATTCAATTATCCAACGAATATCACCAGCTTGCCTGGTCTTGTAAGAATGAT
TAGAAAATTTGGTATTTTGGTATTTAAAAGAATGGTAGAATTGCGCTAATATAAAGTGTAAAGCTATTT
AAAAATAGTCCAAAAACGTAAGGTAGATGAAGTGGAAAGTATTGTAGTTTTTAAAAACGCTATGGTAT
GTGAGGAAGATTTCTATAAATATGTAATTTAACATTTAAGAAGTATTAGTTTTGACCATGAGTGATA
GACATTTCAACTAAGTCGCAATAGATGGTTTCTTGTGAGTAAACAGACATGGCAATTGATTTGCATACG
TGCACCTTGATTGAGCCCTAAACAAGCATCAGTAGTTTGGATCCTTGGAACGTGTCCTATGTGCAACTC
CCGCCCGCATCTACTCCTCCCTCCAGACTTCCGGTGCTGGTTTTTCTAAGCTAAACAGATGTGGGAACA
ACACGTTTCGCACAGGTGTTTGCATGCCACTGCAACACGGGGCGTATGAGTGCTGCCTCCACTTCCATC
ATTTTCGAGCGTAATCATCATCCCGAGGCGTTGACGCAGAACAATTGCCTTAGCCTCCGCCATTTTCAG
CTAATAGAAAACAATTGTGTGTCGCGTAAACGTATTAGGGTACCATTAAGACGCCTGCTTGGATGCGAT
TTAAAATGGTAACACCGCCGCTAGCCAGAA
GGCCAAGTACAACCTCATTATGCATAACTTTGCCAGGGCAACGCCATCATCAGCGAATGGCAATCA
GGCACGTAGCATTAAAGATCATTACACTTAATCAAATCAGTGG
```

3' Homology arm:

```
CCGACATGAGACAACGACACTGGACCCTGACCACAAGCGGCGGAATCGTTTCTGTTACCCAAAAAGC
ACAACACTATTTTACGCTCTTACGACATAATTATGTAACGTAATCGATGGAAACTCAGAACTATACTCAA
TTGGAAGCTCTAGTTTCATTAATATCCAATGTCCAATGTTTCTATGCAACAAAAAATCGAATAC
ATATTTGTAAATACTCAAAGACCCTCGAAATGTTCTGAAAGTTAAACCCTTGGTTTTGATTTAATTCGTA
CTCTTTATTTGCTGAGTGTATAAAGAACTAATAATACGTATTTCAACGATGTTTAAATATCTCACACATA
TTTCCCTAGCATGAAGCACTATTATAAATAACCAACAATGTTTTCAAATCCAAACACTATTTCCGTTG
TATACTTTAATAAAGACAAACTTTTCTCTCAATTTGTGAATGCATAGCAAAATGCAATTGAAATGGTTT
ACATTTAATAGGAAAGTTGGGCTACTCTTTGAACAACATTCAACAACAATGATTTTGGCGAGTTAGATT
GTGAACTTCATACATAATTAACTTTTTCTCTTCTAACAAGTTTATATAGTCAATCACCATGGAATAA
ACAATAAAAAAAGGTACGAAATTTTTTTTACATTTAATTTATTACTGTTGACGGTTTCTTATACGTTAA
AACATTCTAATAAAGTCAATTTTACTAAATGGATTATTGACGCTATTGCATTTTGTGTACGTCATTTGCG
TAATCTTTGAAAAATTTCCGAATTTTATTCGTATCCTTGAATATAATTTTCGTATGAGAATGGTTAATG
GGTCCATAGTACGCAGATATTTTCGCTCCATTGGGTTTTTGTATTTCAATTTTTTGTCTTTGCTGAAA
AAGTTAAAAGTTACCATTTAATTGCATGTTTTTATAAATTTTGGCATTCTAAAGGTTTTATTTAAAT
TAATAAAAAATTAACAATAACAGAATATTCTAAATCAAATGGACAGAAAAACGTGAAATAATGCAG
TTATTATTCATAAATGTCTAGACTTGCAAATTAATAATTTGTATGACTTTTAAAAATTAGTTTCTTTGTCT
GATTCTCATTACATATTGCC
```

#### Generation of *Ms*<sup>TGEM</sup>-*Gal4* mutant/driver line

The *Ms*<sup>TGEM</sup>-*Gal4* mutant line was made by inserting a Trojan Gal4 Expression Module (TGEM<sup>72</sup>) into a PAM site (GTAATTGATAAGTAATCTTGAGG) within intron 3 of the *Ms* gene using CRISPR/Cas9. To make the TGEM construct, homologous arms of approximately 700bp flanking the Cas9 cleavage sites were synthesised by Integrated DNA Technologies, Inc (Coralville, Iowa, USA) and were cloned into the *pT-GEM(1)* vector. The resulting *pT-GEM(1)-Ms* plasmid was co-injected with a *pBS-U6-sgRNA-Ms* plasmid encoding the guide RNA into embryos of flies expressing germline Cas9. Transformants were identified by their expression of the 3xP3-RFP marker.

5' homology arm:

ATTTTCGAGCGTAATCATCATCCCGAGGCGTTGACGCAGAACAAATTGCCTTAGCCTCCGCCATTTTCAG  
CTAATAGAAACAAATTGTGTGTCGCGTAAACGTATTAGGGTACCATTAAGACGCCTGCTTGGATGCGAT  
TTAAATGGTAACACCCGCCGCTAGCCAGAAGGCCAAGTACAACCTCATTATGCATAATACTTTGCCAG  
GGCAACGCCATCATCAGCGAATGGCAATCAGGCACGTAGCATTAAAGATCATTACACTTAATCAAAATCA  
GTGGGGTTGGATGGGCATGGGGCATGTAGCATGGAGCGTGGAGCTTGGCTTAGTCGCCCTCCAGCCA  
GGATGTCCTTGCCGCGCAACCTTTGCCGGCGATAATCAAATAAGCTCGACACCAGCTTTGCTTGTCAAT  
CATGTTTCATAACCCACTTGCAGCATGTCCTTCGCTCAGTTCTTTGTCGCCTGCTGCCTGGCCATCGTCT  
CCTGGCCGTGTCCAACACACGGGCCGAGTCCAGGGTCCACCTCTATGCCAGTCTGGCATCGTCGAGG  
AGATGCCCCGCACATCCGGAAGGTGTGCCAGGCCCTGGAGAACTCCGATCAACTGACGTGGCGCTG  
AAGTCTACATCAACAACGAGGCATCCGGTGAGTGAATCAGGACCAGAGAATTTACCT

3' homology arm:

TAAGATTACTTATAAATACTATGCTTGCTCCAGCTTTGGTGGCCAACTCTGATGACCTGTTGAAGAACT  
ACAACAAGCGAACGGATGTCGATCACGTCTTCTGCGTTTCGGAAAACGTCGTTAAGGACATTTTTTTG  
CAAGGACATCCCGAACACCACTTGGTCGCGACATGAGACAACGACACTGGACCCTGACCACAAGCGGC  
GGAATCGTTTCTGTTACCCAAAAAGCACAACACTATTTTACGCTCTCAGCATAATTATGTAAACGTAA  
TCGATGGAACTCAGAACTATACTCAATTGGAAGCTCTTAGTTCATTAAATATCCAATGTCCAATGTTT  
CTATGCAACAAAAAATAATCGAATACATATTTGTAAATACTCAAAGACCCTCGAAATGTTCTGAAAGT  
TAAACCCTTGGTTTTGATTTAATTCGTACTCTTTATTTGCTGAGTGTATAAAGAATAATAATACGTATT  
TCAACGATGTTTAAATATCTCACACATATTTCCCTAGCATGAAGCACTATTATTAATAACCAACAAATG  
TTTTCAAATCCAACACTATTTTCCGTTGTATACTTTAATAAAGACAAACTTTTCTCTCAATTTGTGAAT  
GCATAGCAAAATGCAATTGAAATGGTTTACATTTAATAGGAAAGTTGGGCTACTCTTTGAACAA

#### Generation of *MsR1<sup>TGEM</sup>-Gal4* mutant/driver line

*MsR1<sup>TGEM</sup>-Gal4* was generated using the method described in<sup>72</sup>. The coding intron flanked by the first two coding exons of *MsR1* locus was targeted for double strand breaks by two different gRNA's (gRNA1: 5'-GGGCTCCAGGTGGGACGTAC-3' and gRNA2: 5'-GAGTCGGCAGAGGTCCGCGG-3'). Similar to *MS<sup>d</sup>*, a two-breaks approach was used to minimise off-target breaks, and the *pCFD4* plasmid (Addgene #49411) was used for gRNA expression. Homology arms flanking the *Cas9* cut sites were subcloned into the *pTGEM(1)* (Addgene #62893) plasmid. Both vectors were injected into *yw; nos Cas9(II-attP40)* flies by BestGene.

5'-Homology arm:

GGCAACATCATAGCCATTAGCTGCTGGCGCAAGGGAACCGTTCAAAAATCGATTATCGCCCCATTTCCG  
GGGAGCTTCTATTTGATTTGCCGTACAATTTCTCGGGCGATTAAACGACGAAGCAGAACGAAAACAA  
AAAACAGATTTGTCAACAGCAAGGTCAACAATTGATGGCTGAAATCAATTTAATTGACCATATCCTACG  
GGCCCTCCAAGTGGCCATCTGCTGCACCTATAAAAAAGTGAATCCGGTCTGCGATTATTTATATATTCGT  
TGCATGGCAGGCGGTCTGTA AAAACCTCGAGATGATGATTA AAAAGCGGCCCTAAAACTTAATGGCGGTT  
TAGGAAATTC AATTCCTGTAATTTAAGCCGAGTCAACATTCTCGAAGTTCTTACATGTAAGCGATAATA  
AATAGTTAAGTCAATTGGCCAATAAACCTATTAATATTGTGCATTTACCACGATTAGACTTTGATTAAAG  
TGACAATGCTGATTTCTGTAGAGGAAATCTAGTTCTAGTCTTCCACAAAGCTATTTAGTTACTCTTGAA  
TAAATATGTTACTTTTCTTTTGCCAAAACCAACAGAATTTTAAATTTAATAATTTGGATTTTTGCAATAA  
ACTGTACTGATTAATGGGCCACACAAAATGTCTAGTTTATTATGGAGCTCTTGGTTTCATAAATTAAGA  
ACATAATCCAATCGGCATATAAATCATTGATAGCAATTTATTTCCGTGATGAAACTGTGCTCCGTGTGA  
ACTGCGAATTA CTATTCTACGGTTGCAAAAAAGCCACCAACGGTCAACATTTAGACCAGGACTTTTA  
GTTTTAATTAGAGCCAGCCTGGCCAACAGCAGTGTAAATGACCACAAAGTGGCTGGCCACAGGATCAG  
CATCCCAGAATGCGATGCCGCATTTGCTTTAATTAAGGTAGTAGCTGGAGTTTGAAAGATGACTGTAT

GGCAATTAGATGTGTAGCCAGAACAACCTTGGCCATTTACTTTTGTGTCAAAGTCGTGCCAAATTGCCAGC  
GGAGGGCGACTTGTACGCTGTACGCCCCAGACAGACGCAGACCGGCCCAAAGCACCCACTCAGCCG  
TCTCCAGGCGCCACTCAAGCGCAAAGGAACGCCAAAACACTAGGACACAGAACGCCAGAAGACTCG  
AAAAAAAAGTAT

3' Homology arm:

CGGCAACGACAACAACGTCGACGACATGAATGAAGTCCTGGAATTGTTTTGCACCAGGATGGCATCGG  
GGCTCCAGGTGGGACGTACTGGCTCAAAGTTATTGGCCCAGAAATCAGGCATAGTTAGCTGCCGAAAT  
GAAACCCAAATACCGAGAAAAGTAGGCAAACAACAGTAGTACACCGGAAATGCATATCATTGTA  
AACTACATCAGTTTACCTAAAAGGCTTGGCTTTAAGCTTTCACATTTATAAAAATATTGAAAATGCATAT  
AAAAGTATGAAATTAATCCCTTTTGTCAATAAACTTTCTTTCTTTCTTTCTGTGTAATATGGGGGATA  
GGTTTTTTTTTTTTTCAATGAAATCCCTTCGAAAGGTATAAGTTCAGAATCGAGAGTTTTATGCCAAGTT  
GGGCACAGTTTTTTTTTCCCAGCTACCTAAAATAATAGAGACATTTTCCCTCCCACTACA  
ACTGATTGCA  
TTGCCGGTGCAGAAAGTTTTTTCAGTTGGTTCGGAAAAATTTGGTTCGCAAACAATTAATATGAACTG  
GCAAGCATTTTTTCGGGCAAAAAGCTCTCATCTATGTAGATTGGAATGGAAATTCGGCTAGAATTGCAT  
AAGACCACCTGCAGTGTGGGCTAACATGACTAAAAAGTTGTCCACAAATTTGGCTTAGATTCTCCAATA  
AACTGTCGTTTCGGCCAGGAATCCCCTTTTTGTTTCGAGTGAATGGGGAATTTTCGCACGACAGACAGC  
AATAAAGAATTTAACTAAAGTCCTGACACCGACAGCACCAGCAGGACGCACACGTGCACTCCATTTGG  
AGAGCTTGGAGTATATTAACATTTTTTCCCACCAGTCAGCCGCAGGACTTGCATCGGTCTCGCCTCGC  
ATTTTCTATATAAATTTTATGCTAAGTCTAATTTGTTGGCTGCAACTTGCACAAAGGCAAAAATAAAC  
AAGGGCGAAATGCCGAAAGCCAAAACCAACCGAAACCGTTGAGGGCTGCCTCGCTTTTTTCTGTGC  
CGAATTCCTAAAACCTTTCACATAAATTTGAGTCCTGCGCCTGGGCTTTTCTCTCCACCT

#### RT-qPCR

RNA was extracted from fly heads in groups of 20 flies using Trizol (Invitrogen). RNA was cleaned using RNAeasy mini Kit (QIAGEN), and cDNAs were synthesized using the Quantitect-QIAGEN reverse transcription cDNA synthesis kit from 500ng of total RNA. Quantitative PCRs were performed by mixing cDNA samples (5ng) with TaqMan Master Mix (ThermoFisher, 4369016) with a commercially available probe of *Ms* (ThermoFisher 4351370 Dm02152471\_g1) as well as a control for *aTub84B* as a control housekeeping gene (ThermoFisher, 4331182 (Dm02361072\_s1). Three biological replicates were used for each sex/mating condition, and each biological replicate consisted of 20 pooled brains. Values were plotted as relative to *aTub84b* expression.

#### Sequence search and phylogenetic analysis

The *Drosophila melanogaster* MsR1 and MsR2 sequences belong to the Pfam domain 7TM\_GPCR\_Srw (PF10324). This domain was used to scan a reference panel of metazoan genomes covering the whole span of metazoan diversity using HMMER3<sup>73</sup>. Given that no sequences for deuterostomes were found using HMMER3, we then used BLASTP to search for MsR1-like amino acid sequences in vertebrate genomes. The resulting 294 sequences from both searches were aligned using MAFFT<sup>74</sup> linsi mode, then trimmed using trimAL<sup>75</sup> in gappyout mode. The trimmed alignment was fed into IQ-TREE<sup>76</sup> using automated mode for model selection and 100 bootstrap replicates to compute nodal support. The resulting tree was rooted using vertebrate sequences as an outgroup.

To search for Sex Peptide, Ms and Mip, we blasted the *D. melanogaster* sequences against metazoan genomes and gathered the best hits of closely related species based on an e-value < 1e-05, aligned them using MAFFT, curated the alignment and used it to build a sequence profile

for HMMER3<sup>73</sup>. These HMMER3 profiles were then used to scan the reference set of metazoan genomes with higher accuracy. Hits for distantly related species were inspected manually to avoid false positives and validated using the reciprocal best hit criterion against *D. melanogaster* genome.

GPCR phylogenetic tree:

[https://www.dropbox.com/s/3wre9qzy6i0uyyo/7TM\\_GPCR\\_Srw\\_phylogeny.tree?dl=0](https://www.dropbox.com/s/3wre9qzy6i0uyyo/7TM_GPCR_Srw_phylogeny.tree?dl=0)

GPCR sequence alignment:

[https://www.dropbox.com/s/ntb0nzx9jutanto/7TM\\_GPCR\\_Srw\\_phylogeny.al.fasta?dl=0](https://www.dropbox.com/s/ntb0nzx9jutanto/7TM_GPCR_Srw_phylogeny.al.fasta?dl=0)

Software versions:

MAFFT v7.221

trimAL v1.4.rev15

HMMER 3.1b2

IQ-TREE 1.5.5

### **Crop model**

To model the effect of crop pumping on food intake, we assumed that the oesophagus, crop duct, and gut are cylindrical tubes (providing some resistance to flow) and that the crop itself is a sphere that can expand and contract (Extended Data Fig. 10h). We then used the Hagen-Poiseuille equation to relate the measured dimensions of the digestive system to the hydraulic conductivity  $K$  in each branch, giving a flow rate  $J = K\Delta P$  where  $\Delta P$  is the pressure drop along the segment and

$$K = \frac{\pi r^4}{8\mu L},$$

where  $r$  the radius,  $\mu$  is the viscosity, and  $L$  the length. Assuming the gut valve is closed when the crop is expanding,  $J_o = J_c = dV_c/dt$ , the volume rate of change of the crop. If we further assume for simplicity that the pressure at the mouth is zero, we find the pressure in the crop

$$P_c = -\frac{dV}{dt} \left( \frac{1}{K_c} + \frac{1}{K_o} \right).$$

Higher flow rates require larger negative pressures in the crop, while higher conductivities mean the same flow can be achieved with smaller negative crop pressure. We measured the dimensions of the oesophagus and crop duct from microscopy to estimate their conductivities, and the sip duration (0.13s) and intake per sip (1.05nL) from<sup>39</sup> to estimate  $dV/dt$  of the crop in mated flies. We calculate that the intake per sip for virgin females is less by a factor of 0.6 based on our own quantifications of sip number and total intake (Supplementary Table 1). The crop pressure required to achieve the measured flow rate from<sup>39</sup> is -1kPa which is comparable to the -0.5kPa to 1kPa measured in cockroach crops<sup>38</sup>, suggesting that crop pumping is a plausible physiological mechanism to drive food intake.

### **Immunohistochemistry and tissue stainings**

Following dissection, the central and enteric nervous systems, gut-associated secretory glands together with intact intestinal tissues were fixed at room temperature for 45min in PBS, 4% paraformaldehyde. All subsequent washes were done in PBS, 4% horse serum, 0.3% Triton X-100 at room temperature following standard protocols. Primary antibody incubations were done at 4°C overnight, whereas secondary antibody incubations were done at room temperature for 2h.

The following primary antibodies were used: rabbit anti-Akh<sup>23</sup>, (1/200), rabbit anti-Burs<sup>77</sup>, (1/200), rat anti-Elav (DSHB, 7E8A10 1/25), mouse anti EcR (DSHB, DDA2.7 1/10), goat anti-GFP (Abcam, ab5450 1/1000), rat anti-IIP2<sup>78</sup>, (1/500), rabbit anti-Ms<sup>79</sup>, (1/1000), mouse anti-Pros (DSHB, MR1A 1/25).

Fluorescent secondary antibodies (FITC-, Cy3- and Cy5-conjugated) were obtained from Jackson Immunoresearch and used at 1/200. Vectashield with DAPI (Vector Labs) was used to stain DNA. Phalloidin stainings were performed after immunohistochemistry using mushroom phalloidin AlexFluor<sup>®</sup> 647 probe (Life Technologies #A22287, 1/200 for 45min).

Custom-made FISH probes were outsourced to either Stellaris RNA FISH (for *Ms* transcript) or Advanced Cell Diagnostics RNAscope (for *MsR* and *Rk* transcripts) fluorescent multiplex assay protocols and reagents. Dissection tools and surfaces were treated with RNaseZAP<sup>™</sup> for single RNA *in situ* stainings, which were generally conducted according to the standard manufacturer's protocol following tissue dissection. For Stellaris probes, dissected samples were dehydrated in 70% EtOH overnight at 4°C. The probes were applied in the hybridisation buffer according to manufacturers' instruction, followed by a 4h incubation at 45°C. Subsequent washes were also performed at 45°C prior to mounting in Vectashield. For RNAscope a negative control probe was provided, targeted against the bacterial gene *dapB*.

For Burs stainings, flies were pre-starved for 22h prior to dissection and immunostaining to maximise retention of otherwise circulating Burs peptide in enteroendocrine cells<sup>36</sup>.

### **Crop and intestinal transit measurements and assays**

Crop size and fullness as well as transit of dye-laced food along the alimentary canal were assessed in response to certain diets, internal states and/or genetic manipulations. Virgin flies of both sexes were collected and aged for either 4 or 7 days when raised at 25°C or 18°C respectively (tipped over to fresh food every 2 or 3 days respectively). Each group of flies was then either mated for 24h or kept as a virgin control group. After mating, flies were either starved overnight (14-16h) or kept feeding *ad libitum* on standard food. The next morning at 11am flies were gently transferred to tubes containing FCF Blue food by a single quick tap and allowed to feed *ad libitum* for 20min if previously starved, or 2hr otherwise. After feeding, flies were transferred by a single quick tap to a fresh empty fly-food vial and euthanised by snap freezing them in liquid nitrogen. Frozen tissues were either used for dissection directly or kept at -80°C (for analysis at a later stage). Tissues were never thawed and re-frozen. Experimental and control flies were all raised and assayed in the same batch of food for each experiment. For temperature-sensitive experiments we devised a simple home-made solution for temperature control that allows for real time monitoring of feeding behaviour. We named this the "sand incubator". This comprised an empty metallic tray for fly vials filled with sand used for pet

reptiles (Zoo Med WC-2 Repti-Sand, 4.5 Kg, Desert White) placed onto a heat mat (Exo Terra Heatwave Desert Heat Mat, 28 x 43 cm, Large). The mat's temperature was controlled by a thermostat (HabiStat. Digital Temperature Thermostat + Timer). Fly vials were immersed in the sand for temperature control remaining available for undisturbed assaying of feeding behaviour. Tissues were dissected in 1.5x PBS (to avoid dye leaking out of the gut through small holes poked during dissection) and were either manually scored for crop size and food location, or transferred to a slide for brightfield imaging immediately after dissection.

#### Crop size and enlargement quantifications

Crop area and roundness measurements were conducted on segmented crops using the Fiji image analysis software. For crop area, we used either the 'Polygon' or the 'Wand' tracing tools, using the 'Default' method in 'Threshold Color' to generate a binary mask that segmented blue-stained crops against a white background. Roundness corresponds to  $4 \cdot \text{area} / (\pi \cdot \text{major\_axis}^2)$ , or the inverse of the aspect ratio.

For crop shape analysis, 2 landmarks and 20 semi-landmarks were annotated for each crop using the 'multipoint tool' in the Fiji image analysis software. Fixed landmarks were assigned to the base of the crop, where it meets the crop duct, and to a point diametrically opposed to this on the crop margin and along the axis of symmetry. 10 semi-landmarks were placed between each fixed landmark and allowed to slide between the immediate 2 neighbouring landmarks. Landmark coordinates were subjected to a Generalized Procrustes Analysis (GPA) to standardize for size, position and orientation, assuming bilateral symmetry. We analysed variation in crop shape using Principal Component Analysis (PCA) of the GPA aligned configurations of crop shapes and visualized these differences using thin plate spline (TPS) deformation grids. All morphometric analysis was performed using the 'geomorph' R package (Adams and Otárola-Castillo, 2013).

For a small subset of experiments (typically those that were confirmatory or negative), crop size was only assessed qualitatively; crop size was ranked as one of four categories: small (S), medium (M), large (L) and very large (VL).

#### *In vivo* crop enlargement assays

For live imaging of crop enlargement, virgin flies were collected and aged for 5 days at 25°C and then either mated for 24h or kept as virgin. Flies were then starved for 2-3h before being briefly anaesthetised on ice (2-5mins) and mounted between two coverslips using a modified version of the Bellymount protocol<sup>80</sup> in that the flies were positioned over the edge of the coverslip to allow access to mouthparts for feeding. Mounting allowed crop and some loops of the midgut to be visible through the ventral surface of the abdomen. Flies were positioned with ventral side up and imaged on a Leica MZ165 FC attached to an S-View SXY-I30 camera. Flies were fed with liquid food containing Brilliant Blue FCF (2g Brilliant Blue FCF, 10g sucrose, 10g yeast extract, 200ml H<sub>2</sub>O) using a narrow capillary for 3-5mins and then were imaged for a further 10mins. Time from first sip to food visible in the crop to food visible in the midgut was calculated.

#### **Food intake and feeding behaviour assays**

##### FlyPAD

FlyPAD assays were performed as described in<sup>39</sup>. Half of the wells of a given flyPAD arena were filled with 2.4µL of food (5% yeast 7% dextrose in 1% agar), and the other half were either loaded

with an agar control (1% agar) or left empty. For all experiments, flies were individually transferred to flyPAD arenas by mouth aspiration and allowed to feed for 1h at 25°C or 29°C and 65% relative humidity. The total number of sips per animal over this hour was acquired using the Bonsai framework<sup>81</sup>, and analysed in MATLAB using previously described custom-written software<sup>39</sup>. Non-eating flies (defined as having fewer than two activity bouts during the assay) were excluded from the analysis. All flyPAD experiments were performed at the same time of the day between 11am and 1pm. Values shown in figures indicate the number of flies tested for each genotype. Data for experimental and control genotypes used for comparison was always acquired in the same flyPAD assay.

#### Blue dye-based assays

Quantification of ingested food was carried out using diets containing 1% Brilliant Blue FCF (Sigma, #807171). Flies were allowed to feed (for up to 20min if pre-starved, and for up to 2h if previously fed *ad libitum*) and were then transferred by a single quick tap to a fresh empty fly food vial for snap freezing in liquid nitrogen. Frozen flies were transferred in groups of three to a clean 2mL PCR tube (Eppendorf, #22431048) with 0.5mL of water and a stainless-steel metal bead 5mm (QIAGEN, #69989). Fly tissues were homogenized using a QIAGEN TissueLyser II for 90sec at 30Hz. The samples were centrifuged at 10.000g for 5-10min. 0.2mL of the supernatant were directly transferred to separate wells of a 96-well, flat bottom, optically clear plate (Thermo Fisher Sterilin, #611F96). A BMG Labtech FLUOstar Omega plate reader was used to measure dye content by reading the absorbance at 629nm. We used a standard curve of pure FCF blue dye to calculate the dye contented ingested per fly.

#### **Fertility and fecundity assays**

Virgin females were raised and aged for 7 days at 18°C, and then shifted to 29°C for the experiment. A group of 40 female flies of each of the three genotypes was used and crossed to 25 *OrR* males. The assays were performed in fly cages on apple juice plates with a smear of live yeast. The number of eggs laid per 24h window was manually counted using a hand-held counter device. To assess egg viability, 200 freshly laid eggs (laid over a 6h window) were collected for each genotype with a hook, split into 10 fresh food vials in groups of 20, and kept at 25°C until eclosion. The number of adults from each tube was scored.

#### **Imaging**

##### Brightfield imaging

Dissected crops and intestines were imaged using either a Leica MZ16F stereomicroscope attached to a DFC420 camera, or a Leica MZ165 FC attached to an S-View SXY-I30 camera. A Leica MZ16F stereomicroscope attached to a DFC420 camera was used for the *in vivo* crop imaging.

##### Confocal imaging

A Leica SP5 confocal microscope was used to generate all confocal images. The images were acquired using both Leica HyD Photon counters as well as standard PMTs tailored for the fluorophores of each sample accordingly. For Flybow clones we used the built-in Leica channel unmixing algorithm post imaging.

##### Quantifications of Ms neuron crop axonal terminals

The number of branches in crop terminals and their diameter were analysed using the NeuronStudio software<sup>82</sup>.

### In vivo calcium imaging

*Ms-Gal4* flies were crossed to *UAS-GCaMP6f (attP40)* to drive the expression of the calcium reporter in Ms neurons. Virgin female flies from the progeny were collected and aged for 4-5 days. Flies were then either mated or kept virgin and used for imaging experiments. Flies were briefly anesthetized (5s) on ice and one fly was picked and glued for surgery. The proboscis was also glued to the thorax to limit motion artifacts during image acquisition. Surgery was performed to open the cuticle and obtain optical access to the brain as described previously<sup>83</sup>. During surgery and subsequent recordings, the aperture on the top of the fly head was bathed in an artificial haemolymph-like solution (130mM NaCl, 5mM KCl, 2mM MgCl<sub>2</sub>, 2mM CaCl<sub>2</sub>, 36mM sucrose, 5mM HEPES-NaOH; pH 7.3; 305mOsm).

Confocal imaging was performed under a scanning confocal microscope (Olympus BX61WI), using a water-immersion 20x objective (XLUMPlanFL, NA 1.0) and an excitation laser at 470 nm. The laser intensity was adjusted for each sample, but on average the laser power was similar between the two conditions (mated and virgin). Fluorescence recordings were performed at a rate of one image every 427ms in a single plane. To collect from the maximum number of cells, multiple planes were recorded consecutively in some samples.

Image analysis was performed offline with a graphical user interface custom-programmed with Matlab. Regions of interest (ROI) were delimited by hand and surrounding individual cell bodies of GCaMP6 expressing cells. Cells were classified as big or small based on expert knowledge of PI Ms neuronal anatomy (D.H.). After background subtraction, the absolute level of the 8-bit encoded fluorescence was calculated for each ROI as the mean over a time period selected for showing minimal fluctuations. Amplitude oscillation measurements were conducted as described in<sup>84</sup>.

### **Cell number quantifications, statistics and data presentation**

For each experiment, a minimum of 10 samples per group was examined per genotype or condition. Experiments were repeated at least 3 times.

Quantifications of fluorescence signal in brains of virgin and mated females and males stained for the anti-Ms antibody was performed using FIJI measurements and the corrected total cell fluorescence (CTCF) metric. The brain samples used for these measurements were raised on the same food batch, dissected at the same time and stained on the same slide. They were then imaged applying the same imaging parameters.

For counts of Ms-positive, *CaLexA* activated cells, flies were dissected and stained 22h after mating along with virgin controls. These flies were raised on the same food batch, dissected at the same time and stained for Ms on the same slide. The same imaging parameters were applied to both groups and Ms- and GFP-positive cells were manually counted upon inspection of the entire brain.

Cell counts of enteroendocrine cells in the intestines of mated and virgin flies were performed 22-48h after mating. These samples were raised on the same food batch, dissected at the same time and stained for Pros and Burs on the same slide. The same imaging parameters were applied. The posterior-most portion of the midgut was imaged using the Malpighian tubules at the level of the hindgut as a posterior-most landmark imaging the entire field of view with in 20x and 63x magnification. The entire dorso-ventral axis was taken into consideration when manually counting cells making use of the Cell Counter plugin in FIJI.

All statistical analyses were carried out in GraphPad Prism 7.04. Comparisons between genotypes/conditions were analysed using Kruskal Wallis and Mann-Whitney-Wilcoxon tests for multiple or pairwise comparisons, respectively, conservatively assuming that data distributions were not parametric (as it is often the case for our data outputs). For egg laying experiments, a two-way ANOVA followed by a Tukey's multiple comparison test was used, considering day and genotype as independent factors. All graphs were generated using GraphPad Prism 7.04. Ranked crop values are displayed as percentages. All confocal and bright field images belonging to the same experiment and displayed together in our figures were acquired using the exact same settings. For visualisation purposes, level and channel adjustments were applied using ImageJ to the confocal images shown in the fig. panels (the same correction was applied to all images belonging to the same experiment), but all quantitative analyses were carried out on unadjusted raw images or maximum projections. In all figures, n denotes the number of samples assayed analysed for each genotype. Data is presented as boxplots with all data points shown and the min and max values plotted, p-values are indicated as asterisks highlighting the significance of comparisons (non-significant (ns):  $p > 0.05$ ; \*:  $0.05 > p > 0.01$ ; \*\*:  $0.01 > p > 0.001$ ; \*\*\*:  $p < 0.001$ ).

## Acknowledgements

We thank Cyrille Alexandre, Julia Cordero, Alex Gould, Bruno Hudry, Matthias Landgraf, Pierre Léopold, Olena Riabinina, Iris Salecker, Liliane Schoofs, Julie Simpson and Yan Zhu for providing reagents. Sophie Austin and Marion Hartl contributed to the early characterisation of crop innervation. Cyrille Alexandre provided valuable assistance with the *Ms* mutant design. We are grateful to Jake Jacobson and Tatiana Lopes for supporting our work experimentally. Chad Whilding assisted with imaging quantifications. Venizelos Papayannopoulos provided valuable comments on the manuscript. This work was funded by an ERC Advanced Grant and a BBSRC grant to I.M.-A. (ERCAdG 787470 'IntraGutSex' and BB/N000528/1, respectively), and MRC intramural funding to I.M.-A.

## Data availability statement

The authors declare that data supporting the findings of this study are available within this manuscript. The datasets generated during and/or analysed during the current study are available from the corresponding author on reasonable request.

## Author contribution statement

D.H. and I.M.-A. designed and conceived the study. D.H. and G.K. performed most experiments and analysed data. P.G. conducted crop enlargement, feeding and fecundity experiments, developed ways to quantify crop enlargement and analysed data. A.M. conducted some immunohistochemistry and fecundity experiments. L.B. conducted immunohistochemistry experiments and acquired and analysed feeding/crop enlargement videos. T.A. conducted some immunohistochemistry and RT-qPCR experiments. C.S. assisted with fecundity experiments, fly husbandry and video recordings. A.d M. performed phylogenetic analyses. A.B. provided the mathematical model. P-Y.P. and T.P. hosted and trained D.H. to perform *in vivo* brain imaging experiments, P-Y.P performed calcium imaging experiments and analysed these data. I.M.-A. wrote the manuscript, with contributions from D.H.

## Competing interests

The authors declare no competing interests.

## Extended data figure legends

### Extended Data Fig. 1. Innervation of the anterior portion of the adult *Drosophila* intestine

**a**, Schematic summary of the innervation of the anterior portion of the adult fly intestine, encompassing foregut, crop and anterior midgut. **b**, Pan-neuronal *nSyb-Gal4* driver expression visualised with EGFP (from *UAS-FB1.1* reporter) in green. Gut muscles are highlighted in blue with phalloidin staining. In all subsequent panels, driver expression is in green and phalloidin staining in blue. Abbreviations are as per **a**. **c**, Cell number quantifications of the enteric nervous system (ENS) ganglia and secretory glands associated with the adult anterior midgut. **d-d''**, Direct innervation of the crop by neurons located in the central nervous system. **d'**, Projections emanating from the insulin-producing neurons in the PI (labelled with *Ilp2-3-Gal4*-driven expression of *UAS-FB1.1*-derived EGFP in green) innervate the crop and anterior midgut. Neuronal nuclei are labelled with anti-Elav antibody in red, and gut muscles are labelled in blue with phalloidin. **d''**, The axonal projections of these insulinergic neurons are visualised using immunostaining for *Ilp2* peptide in red. **e-e''**, Innervation of the crop by peripheral neurons. Taste receptor-expressing neurons visualised with the *Gr43a<sup>KI</sup>-Gal4* driver; gut muscles are labelled with phalloidin. The boxed area in **e'** highlights the cell bodies of ENS-like sensory neurons located in the HCG. **e''** shows the axonal terminals of the same sample on the crop muscle lobes (arrow). In **d-e''**, arrowheads point to the paired nerves innervating the crop. **f-j**, Spatially restricted *Gal4* drivers or antibodies reveal distinct crop-innervating neuronal subsets. In all panels, *Gal4* expression is visualised with EGFP (from *UAS-FB1.1* reporter) in green, and gut muscles are highlighted in blue with phalloidin staining. **f**, *Dh44-Gal4* expression. *Dh44-Gal4*-positive cell bodies in the PI (top dashed box) project to the HCG (bottom dashed boxed) and crop through the crop nervi. They also innervate the anterior midgut. No *Dh44-Gal4*-positive cell bodies are apparent in the HCG. DAPI labels the nuclei of the brain-gut axis in cyan. **g**, *Mip-Gal4*-positive cell bodies are found in both the PI and HCG (dashed boxes). Axons project to the anterior midgut, and along the crop nervi towards the crop. **h**, Glucagon-like Akh peptide (labelled with an anti-Akh antibody in red) is produced by cell bodies located in the paired *corpoca cardiaca* (CC) glands and is apparent in their projections along the crop nervi up to the junction between crop duct and lobes. **i**, Expression of a *pain-Gal4* reporter for *painless* (coding for a TRPA channel mediating detection of noxious heat and mechanical stimuli) in a subset of ENS neurons in the HCG (dashed box), pointing to possible mechanosensory identity. **j**, Expression of a *Gr28a-Gal4* reporter for *Gustatory receptor 28a* in two HCG cell bodies (dashed box), suggestive of chemosensory identity. Their neurites populate the anterior midgut and their axons project along the recurrent nerve (RN). **k**, The *Aug21-Gal4* reporter reveals short local projections from the *corpus allatum* around the foregut and anterior midgut. **l-m**, The use of Hox gene reporters allows labelling of large population of central neurons in thoracico-abdominal ganglion segments. No neurons in the *Ubx-Gal4* (**l**) or *abdA-Gal4* (**m**) expression domains contribute to the innervation of the crop of anterior midgut. *Gal4* expression is visualised with EGFP (from *UAS-FB1.1* reporter) in green, and gut muscles are highlighted in blue with phalloidin staining. Neuronal nuclei are visualised in red with anti-Elav (SG = salivary gland). Scale bars = 50µm. Sample sizes: **b,d-m** = 10-15, **c** = 20. See Supplementary Information for a list of full genotypes.

**Extended Data Fig. 2. Intestinal transit dynamics and dietary regulation of crop enlargement**

**a**, Cartoon summarising *ad libitum* and starvation/re-feeding assays using dye-laced food. **b-c'**, Transit of dye-laced food, intestinal transit at specific time points after ingestion. **b**, Gut dissected 10 seconds after feeding initiation; food is apparent in the crop duct and begins to enter the crop. **b'**, Gut dissected 40 seconds after feeding initiation; food fills the crop duct, crop, and begins to enter the midgut. **b''**, Gut dissected 2 minutes after feeding initiation; food fills the crop, crop duct and midgut. **b'''**, Gut dissected 40 minutes after feeding initiation; food fills the crop, crop duct, midgut and has now reached the hindgut and rectal ampulla. All panels show dissected adult fly intestines, anterior (left) posterior (right). **c,c'**, Frequency histogram derived from *in vivo* food ingestion videos (see Supplementary Video 1 for a representative example) showing higher number of flies with faster transit times of food to the crop (**c**) compared to midgut (**c'**). **d**, Quantification of crop area revealed that re-feeding after starvation results in larger crops than *ad libitum* feeding. **e-e''**, Representative dissected guts of a starved fly (**e**, 16h starvation on 1% agar), starved-refed fly (**e'**, 16h starvation on 1% agar, refed for 20min on dye-laced standard food), *ad libitum*-fed fly (**e''**, fed on dye-laced standard food for 2h). **f**, Ability of different food sources to elicit crop enlargement. These are categorized as palatable (P) and/or nutritious (N) using filled boxes if true and empty boxes if false (see Methods for further details of the different diets). In this and all subsequent ranked data panels, crop size was ranked as one of four categories: small (S), medium (M), large (L) and very large (VL). Graphs are colour-coded from light to dark shades of red corresponding to increasing size of the crop. Data are displayed as percentages. Scale bars = 500µm. Sample sizes: **b-b'''** = 10-12, **c-c'** = 24 **d** = 18, **e-e''** = 23-20 and **f** = 27-31. See Supplementary Information for a list of full genotypes.

**Extended Data Fig. 3. Characterisation of Ms expression**

**a**, Cartoon depicting Ms neuronal subtypes. Dashed boxes highlight the main sites of Ms expression: cell bodies in the PI, cell bodies and neuronal projections in the HCG and neuronal projections on the crop muscles. **b,c**, Single-cell Flybow clones of *Ms-Gal4*-expressing neurons (in red); gut muscle labelled with phalloidin (in blue). **b**, The PI and HCG where the Ms cell bodies reside are boxed. No Ms neurons have been labelled in the PI, but a single-cell, mCitrine-positive clone (in red) reveals an HCG neuron that innervates the crop muscle. Inset shows a single-cell clone of a second type of HCG *Ms-Gal4*-expressing neuron that only extends local projections. **c**, Single-cell clone of a PI *Ms-Gal4*-expressing neuron. The main projection bifurcates, with one shorter (putatively dendritic) branch projecting towards the suboesophageal zone (SEZ) (empty arrows), and a longer (axonal) branch projecting towards the midgut/crop (arrows). **d,d'**, Co-expression of the dendritic marker DenMark (in red) and membrane marker Venus shown (in green) from *Ms-Gal4* reveals relative DenMark enrichment in their SEZ projections (**d**), consistent with dendritic nature. Venus enrichment is apparent in the crop nerve (**d'**), consistent with its axonal identity. Top left arrow points to the crop nerve, and bottom arrow points to where it terminates. **e**, Quantification of fluorescence for DenMark and Venus in SEZ (top) crop nerve (bottom) projections. **f-j''**, *Ms-Gal4* expression, visualized by EGFP from the *UAS-FB1.1* reporter (in green). **f**, Overview of *Ms-Gal4*-positive intestinal innervation; *Ms*-positive neurites are apparent on the crop, anterior midgut and posterior hindgut (rectal ampulla). Neuronal nuclei are stained with an anti-Elav antibody in red, and gut muscles are labelled in blue with phalloidin. **g**, *Ms-Gal4* expression in heart-innervating neurons; heart muscles are labelled in blue with phalloidin. **h**, *Ms-Gal4* expression in peripheral neurons that innervate the ovaries, oviduct and spermatheca (SP). **i-i''**, Co-expression of *Ms-Gal4* and Ms peptide (in red) in a cluster of PI neurons; arrows and arrowheads point to big and small PI Ms neuron subtypes, respectively. **i** and **i'** show single channel images for *Ms-Gal4* and anti-Ms antibody, respectively. The merged image is shown in **i''**. **j-j''**, Co-expression of *Ms-Gal4* and Ms transcript (visualised

using FISH in red) in the same cluster of PI neurons. **j** and **j'** show single channel images for *Ms-Gal4* and *Ms* transcript, respectively. The merged image is shown in **j''**. **k-k'**, *Ms* protein reporter expression (in green). *Ms* peptide is in red and gut muscles are labelled with phalloidin in blue. **k**, Co-expression between the *Ms* protein reporter *Ms* peptide in the nervous system, and in neuronal projections towards the gut. *Ms* and the *Ms* protein reporter are co-expressed by the PI *Ms* neurons (boxed and inset). **k'**, The *Ms* protein reporter also labels axonal projections innervating the crop muscles. **l-q''**, Expression (or lack thereof) of neuropeptides and other markers in the *Ms*-expressing neurons in the PI or HCG. For each letter, the first panel shows double staining, the second and third panels show single channels for clarity. **l-l''**, PI *Ms* neurons do not co-express *Ilp2*, used as a marker of insulin-producing neurons. **m-m''**, PI *Ms* neurons do not co-express *Dh44-Gal4*, used as a marker of Diuretic Hormone 44-producing neurons. **n-n''**, PI *Ms* neurons do not co-express *Mip-Gal4*, used as a marker of Myoinhibiting peptide precursor-producing neurons. **o-o''**, Co-expression between *Ms* and *Mip-Gal4* in 3 out of the 5 HCG *Ms*-expressing neurons. Phalloidin was used to label gut muscles (in blue). **p-p''**, A subset of PI *Ms* neurons co-express *Taotie-Gal4*; other *Taotie-Gal4*-positive PI neurons are *Ms*-negative. In the HCG, *Taotie-Gal4* expression is only apparent inconsistently in one *Ms* neuron (data not shown). **q-q''**, PI *Ms* neurons do not co-express *Dsk-Gal4*, used as a marker of Drosulfakinin-producing neurons. Scale bars: **b, d', f-h** and **k-k'** = 50 $\mu$ m, **i-j'', l-o''** and **q-q''** = 25 $\mu$ m, **b** (inset), **c, d, p-p''** = 20 $\mu$ m and **k** (inset) = 10 $\mu$ m. Sample sizes: **b-d'** = 10-25, **e** = 2 and **f-q''** = 10-15. See Supplementary Information for a list of full genotypes.

#### Extended Data Fig. 4. *Ms* neuron regulation of crop enlargement

**a-a'**, Validation of *Ms<sup>Δ</sup>* mutant using anti-*Ms* staining shown in green; PI is highlighted by dashed lines. **a**, Lack of *Ms* staining in the PI of *Ms* mutants (*Ms<sup>Δ</sup>/ Df(3R)Exel6199*). *Ms* staining is apparent in the PI of *Df(3R)Exel6199* (**a'**) and *Ms<sup>Δ</sup>* (**a''**) heterozygous control flies. **b**, Quantifications of crop area in *ad libitum*-fed flies upon *Ms-Gal4*-driven *TrpA1* expression (4h at the permissive temperature), showing these have significantly larger crops relative to *UAS* and *Gal4* controls. **c**, Quantifications of crop area in starved-refed flies upon *Ms-Gal4*-driven *Kir2.1* expression (temporally confined with *tub-Gal80<sup>TS</sup>*), showing these have significantly smaller crops relative to *UAS* and *Gal4* controls. **d-e''**, Effect of neuronal activation and *Ms* downregulation on *Ms* levels in PI neurons. Thermogenic activation of *Ms* neurons in *ad libitum* fed flies depletes *Ms* peptide (in red) from *Ms* neuron cell bodies in the PI (**d**) compared to *UAS* (**d'**) and *Gal4* (**d''**) controls. Adult-specific *Ms* downregulation in *Ms* neurons of starved-refed flies results in reduced *Ms* staining (red) in PI neurons (**e**), compared to *UAS* (**e'**) and *Gal4* (**e''**) controls. **f-i**, Effect of *Ms* loss-of-function and adult-specific *Ms* neuron inactivation on crop expansion and shape, upon starvation-refeeding in mated females. **f**, Quantifications of crop area revealed that *Ms* neuron inactivation results in smaller crops relative to *Ms* mutant or *w<sup>1118</sup>*, *UAS* and *Gal4* controls. **g**, Representative crop images of genotypes quantified in **f**. **h**, Quantifications of crop roundness revealed that crops are less round upon *Ms* neuron inactivation or in *Ms* mutant compared to *w<sup>1118</sup>*, *UAS* and *Gal4* controls. **i**, PCA of landmark position variation along the crop outline, showing that crop shapes are distinct between *Ms* mutant (red), *Ms* neuron inactivation (yellow) and *w<sup>1118</sup>* (grey), being more similar between *Ms* mutant and *w<sup>1118</sup>*, as highlighted by partial overlap of their 95% confidence ellipses. Wireframe deformation grids are shown to illustrate the minimum and maximum shape deviations as compared to the mean shape along each PC axis. **j-k**, Effect of *Ms* neuron activation on crop expansion in *Ms* mutant background, upon starvation-refeeding in mated females. **j**, Quantifications of crop area show that activation of *Ms* neurons by *Ms-Gal4*-driven *TrpA1* expression resulted in larger crops relative to activation of *Ms* neurons by *Ms<sup>TGEM</sup>*-driven *TrpA1* expression in an heteroallelic mutant background, as well as relative to *Ms* mutant or *UAS* and *Gal4* controls. **k**, Representative crop images of genotypes quantified in **j**. **l-m**, Effect of *Ms* and *Taotie* neuron activation on crop enlargement, upon starvation in mated females. **l**,

Quantification of crop area shows that activation of either Ms neurons or *Taotie* neurons resulted in larger crops compared to respective *Gal4* controls and *UAS* control, even in the absence of food. **m**, Representative crop images of genotypes quantified in **l**. Scale bars: **a-a'** = 10µm, **d-e''** = 25µm, **g, k** and **m** = 500µm. Sample sizes: **a-a'** = 10-15, **b** = 10-15, **c** = 26-31, **d-e''** = 10-15, **f-i** = 28-32, **j-k** = 26-31, **l-m** = 20-27. See Supplementary Information for a list of full genotypes.

#### Extended Data Fig. 5. Expression of Ms receptors and their regulation of crop enlargement

**a**, FB1.1-derived EGFP reveals *MsR1* expression in the crop muscles and nervous system, including nerves innervating the crop, hindgut and rectal ampulla. In this and subsequent panels, muscles are labelled with phalloidin (in blue). **b-b''**, Co-expression between *MsR1* mRNA stained with FISH (**b,b'**, in red) and FB1.1-derived EGFP driven by *MsR1<sup>TGEM</sup>-Gal4* (**b,b''**, in green) is observed in crop muscles. Muscle nuclei are shown in blue with DAPI; single channels are shown for clarity. **c**, Detail of the HCG and *corpora cardiaca* (CC); the latter is extensively innervated by *MsR1*-expressing neurons. **d**, FB1.1-derived EGFP reveals *MsR1* expression in neurons innervating the female reproductive system, but not in its muscles. **e**, FB1.1-derived EGFP reveals *MsR1* expression in heart-innervating neurons, but not in heart muscles. **f**, Higher magnification image of the central brain; nuclear GFP reveals broad *MsR1* expression in neurons including the PI Ms neurons shown with Ms staining (in red). **g**, A subset of 2-3 *MsR1*-positive neurons in the HCG co-express Ms. **h**, Nuclear GFP reveals *MsR1* expression overlaps with Akh staining in CC cells (in red). **i**, Quantification of *MsR1* mRNA levels in various gut regions relative to whole gut levels, showing highest expression levels in the crop (data from Flygut<sup>85</sup>). Intestinal and neuronal expression are also consistent with FlyAtlas data<sup>86</sup>). **j-j'**, Validation of adult-specific *MsR1* knockdown in visceral muscles (*vm<sup>TS</sup> > MsR1-RNAi*). Panels show high magnification images of crop muscles. *MsR1* mRNA expression is visualised by RNA FISH (in green) in *vm-Gal4<sup>TS</sup>* (**j**), but it is reduced/absent from *MsR1* knockdown crops (**j'**). **k**, Quantifications of crop area in starved-refed flies upon downregulation of *MsR1* in visceral muscles, showing that crop size is visibly reduced upon *MsR1* downregulation compared to *UAS* and *Gal4* controls. **l**, A similar reduction in crop area is also quantified upon *MsR1* downregulation specifically in crop muscles using a different driver line (*MsR1<sup>crop</sup> > MsR1<sup>RNAi</sup>*). **m-o''**, Effect of crop muscle-specific downregulation of *MsR1* on crop size. **m**, Quantifications of crop area in starved-refed mated females shows that crop-specific downregulation of *MsR1* (*MsR1<sup>crop</sup> > MsR1<sup>RNAi</sup>*) resulted in reduced crop areas, similar to Ms neuron inactivation (*Ms > Kir2.1*) and significantly reduced as compared to *Gal4* and *UAS* controls. **n-o''**, Representative crop phenotypes of the genotypes quantified in **i**. **p**, Quantification of crop area upon visceral muscle-specific *MsR1* and *MsR2* downregulation, showing that *MsR1* knockdown, but not *MsR2* knockdown, resulted in reduced crop sizes, as compared to *UAS* and *Gal4* respective controls. **q**, Quantifications of crop area in starved-refed mated females shows that heteroallelic *MsR1<sup>TGEM</sup>/Df<sup>Aprt-32</sup>* mutants have reduced crop areas relative to *w<sup>1118</sup>* or heterozygous controls. **r**, Representative crop images from genotypes quantified in **q**. **s**, Validation of *MsR1* mutation and *MsR1* FISH signal specificity. *MsR1* mRNA (green) is absent from the crop muscle cells of *MsR1<sup>TGEM</sup>* mutants, and apparent in *w<sup>1118</sup>* control flies. Scale bars: **b-b''**, **f, g, h, j, j'** and **s** = 10µm, **a, c, d, e** = 50µm, **r** = 500µm and **n-o''** = 1mm. Sample sizes: **a-h, j-j'** and **s** = 10-15, **k** = 22-24, **l** = 27-29, **m-o''** = 28-32, **p** = 31 and **q-r** = 13-15. See Supplementary Information for a list of full genotypes.

#### Extended Data Fig. 6. Post-mating modulation of Ms neurons

**a-b**, Analysis of Ms neuron crop terminals in virgin and mated females. Neither the number of axonal branches (**a**) nor their diameter (**b**) is significantly different between virgin and mated females. **c-g**, Comparison of Ms peptide levels in the cell bodies of PI neurons in fed versus starved virgin and mated females. Representative images of Ms staining in the cell bodies of the PI neurons of fed virgin females (**c**), starved virgin females (**d**), mated fed females (**e**) and starved

mated females (**f**). **g**, Quantification of Ms staining in the cell bodies of PI neurons shows that Ms levels are reduced in mated females compared to virgins, irrespective of fed or starved status. **h**, RT-qPCR expression data for *Ms* transcript levels in the brain of *ad libitum*-fed, control males (grey column), virgin females (pink column) and mated females (red column). No significant differences are apparent between groups. **i-k**, CaLexA-based assessment of mating-triggered changes in PI MS neuronal activity, achieved by adult- and Ms-confined CaLexA expression ( $Ms^{TS} > CaLexA$ ). Representative images of *ad libitum*-fed, wild-type virgin (**i'-i''**), and mated females (**j-j''**) are shown. Ms neurons are labelled with anti-Ms antibody (in red) and CaLexA channel is shown as a single channel (in green), for clarity. **k**, Quantification of CaLexA-derived GFP-positive cells in PI Ms neurons of virgin (pink box) and mated (red box) females, showed that fewer cells are CaLexA-positive in virgin compared to mated females; each data point corresponds to a different brain. **l**, Quantification of baseline GCaMP fluorescence (corrected for background) in Ms neurons of virgin females (pink box) and mated females (red box). Each data point corresponds to an individual cell measurement. Higher GCaMP signal is detected in mated females. **m-n**, Effects of sex and mating status on Ms signalling contribution to crop size. **m**, Quantification of crop area upon adult-specific downregulation of *MsR1* in visceral muscles shows that this was significantly reduced in mated females but not in males or virgin females, as compared to respective controls. **n**, Representative crop images of genotypes quantified in **m**. Scale bars: **c-f** and **i-j'** = 20 $\mu$ m and **n** = 500 $\mu$ m. Sample sizes: **a-b** = 15-19, **c-g** = 12-15, **h** = 3 (each point corresponds to 15 pooled samples), **i-k** = 17, **l** = 19-25 and **m-n** = 15-29. See Supplementary Information for a list of full genotypes.

#### Extended Data Fig. 7. Ecdysone modulation of Ms neurons and crop size

**a-a'**, Expression of EcR in PI Ms neurons. Ms staining (in green) (**a**) and EcR staining (in red) (**a'**) overlap and are shown as single channels for clarity. **b-d**, Ecdysone effect on Ms levels in PI neurons. Representative images show comparable Ms levels upon expression of *EcR<sup>DN</sup>* in virgin females (**b**) relative to *UAS* (**b'**) and *Gal4* (**b''**) controls. Fluorescence signals are pseudo-coloured; high to low intensity is displayed as warm (yellow) to cold (blue) colours. **c**, Quantification of Ms staining intensities in PI neurons of virgin females upon expression of *EcR<sup>DN</sup>* showed comparable levels to *UAS* and *Gal4* controls. **d**, Quantification of Ms staining intensities in PI neurons of mated females upon expression of *EcR<sup>DN</sup>* showed increased Ms levels relative to *UAS* and *Gal4* controls. **e**, Quantification of crop area in starved-refed mated females revealed smaller crops upon adult- and Ms neuron-specific *EcR* downregulation compared to *UAS* and *Gal4* controls. **f-j**, Classification of crop size upon expression of *EcR<sup>DN</sup>* (**f-g**) or *EcR* downregulation (**h-j**) in starved-refed female flies. Distribution of crop sizes did not significantly change relative to *UAS* and *Gal4* controls in virgin females (**f**, **h**, **j**). In mated females, the distribution shifted towards smaller crop sizes, relative to *UAS* and *Gal4* controls (**g**, **i**). Ranked data are displayed as percentages. Scale bars = 20 $\mu$ m. Sample sizes: **a-a''** = 10, **b-c** = 22-24, **d** = 26-29, **e** = 20-24, **f** = 47-49, **g** = 55-68, **h** = 42-51, **i** = 30-43, **j** = 42-52. See Supplementary Information for a list of full genotypes.

#### Extended Data Fig. 8. Bursicon modulation of Ms neurons

**a**, Co-expression of Burs (**a'**, in red), Pros (**a''**, in white) and GFP driven by *Tkg-Gal4* (**a'''**, in green) in midgut enteroendocrine cells of mated females. **b**, Quantifications of Pros-positive midgut cells shows increased enteroendocrine cell number in mated females relative to virgins. Flies were starved for 22h to increase Burs staining in the enteroendocrine cell bodies<sup>36</sup>. Single channels for each marker are shown for clarity. **c**, Quantification of enteroendocrine cells of mated females labelled by *Tkg-Gal4*-driven EGFP and Burs staining (such as that shown in **a**). More *Tkg-Gal4*-positive than Burs-positive enteroendocrine cells are apparent. The majority of Burs-positive enteroendocrine cells are *Tkg-Gal4*-positive. **d-e**, Co-expression of *rk<sup>TGEM</sup>* (driving *FB1.1*, in green) with Ms peptide (in red) is shown in brain and VNC neurons (**d**), and in the HCG

ganglion (e). **f-f'**, Co-expression of  $rk^{TREM}$  (driving FB1.1-derived EGFP, in green) with Ms peptide (in red) was observed brain PI neurons. **f'**, Ms staining is shown as a single channel for clarity. **g-g'**, Co-expression of *Ms-Gal4* (driving FB1.1-derived EGFP, in green) with *rk* mRNA (stained with FISH, in red) was observed in brain PI neurons. **g'**, *rk* mRNA FISH is shown as a single channel for clarity. **h**, Co-expression of  $rk^{TREM}$  (driving FB1.1-derived EGFP, in green) with Ms peptide (in white) and EcR (in red) was observed in brain PI neurons. **i**, Co-expression of *Taotie-Gal4* (driving FB1.1-derived EGFP, in green) with EcR (in red) was observed in brain PI neurons. Nuclei are stained with DAPI (in blue). **j-j'**, Co-expression of *Taotie-Gal4* (driving FB1.1-derived EGFP, in green) with *rk* mRNA (stained with FISH, in red) was observed in brain PI neurons. Nuclei are stained with DAPI (in white). **j'**, *rk* mRNA FISH is shown as a single channel for clarity. **k-m**, *rk* regulation of Ms levels in PI neurons. Representative images show similar Ms staining signal upon adult-specific *rk* downregulation in virgin females (**k**) relative to *UAS* (**k'**) and *Gal4* (**k''**) controls. Fluorescence signals are pseudo-coloured; high to low intensity is displayed as warm (yellow) to cold (blue) colours. **l**, Quantification of Ms staining intensities in PI neurons of virgin females upon adult-specific *rk* downregulation showed comparable levels to *UAS* and *Gal4* controls. **m**, Quantification of Ms staining intensities in PI neurons of mated females upon adult-specific *rk* downregulation showed increased Ms levels relative to *UAS* and *Gal4* controls. **n**, Quantification of the amplitude of GCaMP oscillations in PI neurons of mated females shows that downregulation of *EcR* and *rk* in Ms neurons significantly increased the amplitude of calcium signal. **o**, Quantification of GCaMP baseline fluorescence levels in PI neurons of mated females revealed that downregulation of *EcR* in Ms neurons significantly reduced GCaMP signal, whereas downregulation of *rk* increased GCaMP signal, both relative to expression of EGFP. Hence, calcium oscillations become virgin-like both upon *EcR* or *rk* downregulation, whereas their effects on overall calcium fluorescence are different. Scale bars = 20 $\mu$ m apart from **a-a''** and **d-e** = 50 $\mu$ m. Sample sizes: **a-a''** = 10-15, **b** = 4 (midguts), **c** = 12 (midguts), **d-j** = 10-15, **k-l** = 15-20, **m** = 20-23 and **n-o** = 8-11. Supplementary Information for a list of full genotypes.

### Extended Data Fig. 9. Post-mating modulation of crop enlargement by Burs and ecdysone

**a-a'**, Classification of crop size upon *rk* downregulation in Ms neurons of starved-reared female flies. Distribution of crop sizes did not significantly change relative to *UAS* and *Gal4* controls in virgin females (**a**). In mated females, the distribution shifted towards smaller crop sizes, relative to *UAS* and *Gal4* controls (**a'**). Ranked data are displayed as percentages. **b-e**, Effect of Burs expression from enteroendocrine cells on crop enlargement in virgin (**b, d**) and mated (**c, e**) females. Representative crop images of *ad libitum*-fed flies virgin females show that crop size was not visibly changed upon downregulation of *Burs* in Pros-expressing enteroendocrine cells (**b**) relative to *UAS* (**b'**) and *Gal4* (**b''**) controls. In mated females, the distribution shifted towards smaller crop sizes (**c**), relative to *UAS* (**c'**) and *Gal4* (**c''**) controls. Quantifications of crop area of genotypes shown in **b-b''** and **c-c''** are shown in **d** and **e** respectively. **f-h**, Thermogenic activation of *Tkg-Gal4*-positive cells (which include Burs-positive enteroendocrine cells but also a very small subset of neurons outside the PI, not shown) resulted in significant reduction of Ms signal in the cell bodies on PI neurons of virgin females, relative to *UAS* and *Gal4* virgin controls. **f-g''**, Representative images of Ms staining in PI neurons of the genotypes quantified in **h**. Reduction of Ms staining is apparent in PI neurons of virgin females upon activation of *Tkg-Gal4*-positive cells (**f**) relative to *UAS* (**f'**) and *Gal4* (**f''**) virgin controls. The difference between activated (**g**) vs control (**g', g''**) flies was not apparent when female flies were mated (presumably because more Ms peptide has been released in controls). Fluorescence signals are pseudo-coloured; high to low intensity is displayed as warm (yellow) to cold (blue) colours. **i-j**, Effect of gut hormone release from enteroendocrine cells on crop enlargement. Representative crop images of *ad libitum*-fed female flies shows that crop size was increased upon thermogenic activation of *Tkg-Gal4*-positive cells (**i**) relative to *UAS* (**i'**) and *Gal4* (**i''**) controls. We note that the *Tkg-Gal4*-positive cells include most Burs-positive enteroendocrine cells as well as a very small subset of

central neurons outside the PI (not shown). **k-l**, Effect of ecdysone and Burs signalling in *Taotie* neurons on crop enlargement after mating. Representative crop images of starved-refed mated females show that, relative to the *UAS GD* control (**k**), downregulation of *EcR* (**k'**) or *rk* (**k''**) resulted in visibly smaller crops. Quantifications of crop area of genotypes shown in **k-k''** are shown in **l**. **m**, Schematic summary of key findings. Post-mating increase in circulating levels of Bursicon and Ecdysone signal via their receptors to Ms-neurons, change their neural activity and lead to crop enlargement. Scale bars **f-g''** = 20µm **b-c''**, **i-i''** = 500 µm and **k-k''** = 1mm. Sample sizes: **a** = 31-38, **a'** = 30-39, **b-b''** and **d** = 14-18, **c-c''** and **e** = 16-22, **f-h** = 17-21, **i-j** = 14-15, **k-l** = 26-29. Supplementary Information for a list of full genotypes.

### Extended Data Fig. 10. Regulation of food intake, fecundity and fertility by Ms neurons.

**a-b**, Mated females increase their food intake. Both the amount of ingested dye-laced food (**a**) and the number of sips per fly (**b**) are increased in wild-type mated females relative to virgins. **c-e**, Regulation of food intake by *MsR1* expression in crop muscles. Quantifications of ingested dye show that downregulation of *MsR1* in the visceral muscles of starved-refed virgin females resulted in similar food intake relative to *UAS* and *Gal4* controls (**c**), whereas downregulation of *MsR1*, but not *MsR2*, in mated females, resulted in reduced food intake, relative to *UAS* and *Gal4* controls (**d**). **e**, Quantification of the number of sips per fly show that downregulation of *MsR1* specifically in crop muscles using an independent driver line also reduced food intake relative to *Gal4* and *UAS* controls in starved-refed mated females. **f**, Quantifications of ingested dye-laced food show that downregulation of *EcR* in Ms neurons of starved-refed virgin females does not significantly affect food intake when compared to *Gal4* and *UAS* controls. **g**, Similarly, quantifications of ingested dye-laced food show that downregulation of *Burs* in Pros-expressing enteroendocrine cells of starved-refed virgin females does not significantly affect food intake when compared to *Gal4* and *UAS* controls (**g**). **h**, In the model, food ingestion from the oesophagus is driven by crop enlargement, which is assumed to be linear during sips and constant in between sips. The observed increase in food intake in mated females compared to virgins can be explained by a decrease in negative pressure from -0.8 kPa to -1.3 kPa (increased suction), leading to an increased intake during sips. **i-j**, Thermogenic activation of Ms neurons (*Ms > TrpA1*) for 4h prior to the transfer of flies from undyed to dye-laced food reduces the mean amount of ingested dye during the course of 1h (**i**), and reduces the mean number of sips per fly over 1h of feeding (**j**) relative to *Gal4* and *UAS* controls. **k-l**, Concurrent thermogenic activation of Ms neurons during feeding of dye-laced food increases the mean amount of ingested dye during the course of 1h (**k**), but has no effect on the mean number of sips per fly over 1h of feeding (**l**) relative to *Gal4* and *UAS* controls. **m-n**, Effect of neuronal activation on the regulation of food intake by *Taotie-Gal4*-positive neurons. Quantification of ingested dye-laced food shows that thermogenic activation of *Taotie* neurons for 4h prior to the switch from undyed to dye-laced food reduced the amount of ingested dye relative to *Gal4* and *UAS* controls over the course of 1h (**m**). By contrast, concurrent activation during feeding of such food increases the amount of ingested dye relative to *Gal4* and *UAS* controls over the course of 1h (**n**). **o, p**, Effect of Ms signalling to crop muscles on fecundity and fertility. **o**, Quantification of eggs layed in 24h by mated females shows that *MsR1* downregulation specifically in crop muscles resulted in significantly fewer eggs layed after 4 days relative to *UAS* and *Gal4* controls. **p**, Quantification of adult progeny produced from a 24h period of egg laying by mated females, shows that *MsR1* downregulation in visceral muscles resulted in significantly fewer progeny relative to *UAS* and *Gal4* controls. Sip number measurements were done over 1h of feeding. Sample sizes: for **a, c, d-g, i, k**, and **m-n** each data point represents the average of 3 flies. **a** = 39, **b** = 29, **c** = 27, **d** = 24-30, **e** = 17-34, **f** = 18-30, **g** = 30, **i** = 12-2, **j** = 28-29, **k** = 24, **l** = 9-11, **m-n** = 24, **o** = 60 and **p** = 10-12. Asterisks highlight significant comparisons across genotypes/conditions. See Supplementary Information for a list of full genotypes.

## References

- 46 Burke, C. J. & Waddell, S. Remembering nutrient quality of sugar in *Drosophila*. *Curr Biol* **21**, 746-750, doi:10.1016/j.cub.2011.03.032 (2011).
- 47 Fujita, M. & Tanimura, T. *Drosophila* evaluates and learns the nutritional value of sugars. *Curr Biol* **21**, 751-755, doi:10.1016/j.cub.2011.03.058 (2011).
- 48 Ribeiro, C. & Dickson, B. J. Sex peptide receptor and neuronal TOR/S6K signaling modulate nutrient balancing in *Drosophila*. *Curr Biol* **20**, 1000-1005, doi:10.1016/j.cub.2010.03.061 (2010).
- 49 Ikeya, T., Galic, M., Belawat, P., Nairz, K. & Hafen, E. Nutrient-dependent expression of insulin-like peptides from neuroendocrine cells in the CNS contributes to growth regulation in *Drosophila*. *Curr Biol* **12**, 1293-1300 (2002).
- 50 Miyamoto, T., Slone, J., Song, X. & Amrein, H. A fructose receptor functions as a nutrient sensor in the *Drosophila* brain. *Cell* **151**, 1113-1125, doi:10.1016/j.cell.2012.10.024 (2012).
- 51 Jenett, A. *et al.* A GAL4-driver line resource for *Drosophila* neurobiology. *Cell Rep* **2**, 991-1001, doi:10.1016/j.celrep.2012.09.011 (2012).
- 52 Asahina, K. & Anderson, D. (ed FlyBase) (2013).
- 53 Tracey, W. D., Jr., Wilson, R. I., Laurent, G. & Benzer, S. *painless*, a *Drosophila* gene essential for nociception. *Cell* **113**, 261-273 (2003).
- 54 Thorne, N. & Amrein, H. Atypical expression of *Drosophila* gustatory receptor genes in sensory and central neurons. *J Comp Neurol* **506**, 548-568, doi:10.1002/cne.21547 (2008).
- 55 de Navas, L., Foronda, D., Suzanne, M. & Sanchez-Herrero, E. A simple and efficient method to identify replacements of P-lacZ by P-Gal4 lines allows obtaining Gal4 insertions in the bithorax complex of *Drosophila*. *Mech Dev* **123**, 860-867, doi:10.1016/j.mod.2006.07.010 (2006).
- 56 Hudry, B., Viala, S., Graba, Y. & Merabet, S. Visualization of protein interactions in living *Drosophila* embryos by the bimolecular fluorescence complementation assay. *BMC Biol* **9**, 5, doi:10.1186/1741-7007-9-5 (2011).
- 57 Park, D., Veenstra, J. A., Park, J. H. & Taghert, P. H. Mapping peptidergic cells in *Drosophila*: where DIMM fits in. *PLoS One* **3**, e1896, doi:10.1371/journal.pone.0001896 (2008).
- 58 Zhan, Y. P., Liu, L. & Zhu, Y. Taotie neurons regulate appetite in *Drosophila*. *Nat Commun* **7**, 13633, doi:10.1038/ncomms13633 (2016).
- 59 Guo, Z., Driver, I. & Ohlstein, B. Injury-induced BMP signaling negatively regulates *Drosophila* midgut homeostasis. *J Cell Biol* **201**, 945-961, doi:10.1083/jcb.201302049 (2013).
- 60 Balakireva, M., Gendre, N., Stocker, R. F. & Ferveur, J. F. The genetic variant *Voila* causes gustatory defects during *Drosophila* development. *J Neurosci* **20**, 3425-3433 (2000).
- 61 Song, W., Veenstra, J. A. & Perrimon, N. Control of lipid metabolism by tachykinin in *Drosophila*. *Cell Rep* **9**, 40-47, doi:10.1016/j.celrep.2014.08.060 (2014).
- 62 McGuire, S. E., Le, P. T., Osborn, A. J., Matsumoto, K. & Davis, R. L. Spatiotemporal rescue of memory dysfunction in *Drosophila*. *Science* **302**, 1765-1768, doi:10.1126/science.1089035 (2003).
- 63 Hudry, B., Khadayate, S. & Miguel-Aliaga, I. The sexual identity of adult intestinal stem cells controls organ size and plasticity. *Nature* **530**, 344-348, doi:10.1038/nature16953 (2016).

- 64 Nicolai, L. J. *et al.* Genetically encoded dendritic marker sheds light on neuronal connectivity in *Drosophila*. *Proc Natl Acad Sci U S A* **107**, 20553-20558, doi:10.1073/pnas.1010198107 (2010).
- 65 Sugimura, K. *et al.* Distinct developmental modes and lesion-induced reactions of dendrites of two classes of *Drosophila* sensory neurons. *J Neurosci* **23**, 3752-3760 (2003).
- 66 Hamada, F. N. *et al.* An internal thermal sensor controlling temperature preference in *Drosophila*. *Nature* **454**, 217-220, doi:10.1038/nature07001 (2008).
- 67 Baines, R. A., Uhler, J. P., Thompson, A., Sweeney, S. T. & Bate, M. Altered electrical properties in *Drosophila* neurons developing without synaptic transmission. *J Neurosci* **21**, 1523-1531 (2001).
- 68 Barolo, S. *et al.* A notch-independent activity of suppressor of hairless is required for normal mechanoreceptor physiology. *Cell* **103**, 957-969 (2000).
- 69 Chen, T. W. *et al.* Ultrasensitive fluorescent proteins for imaging neuronal activity. *Nature* **499**, 295-300, doi:10.1038/nature12354 (2013).
- 70 Sarov, M. *et al.* A genome-wide resource for the analysis of protein localisation in *Drosophila*. *Elife* **5**, e12068, doi:10.7554/eLife.12068 (2016).
- 71 Baena-Lopez, L. A., Alexandre, C., Mitchell, A., Pasakarnis, L. & Vincent, J. P. Accelerated homologous recombination and subsequent genome modification in *Drosophila*. *Development* **140**, 4818-4825, doi:10.1242/dev.100933 (2013).
- 72 Diao, F. *et al.* Plug-and-play genetic access to drosophila cell types using exchangeable exon cassettes. *Cell Rep* **10**, 1410-1421, doi:10.1016/j.celrep.2015.01.059 (2015).
- 73 Eddy, S. R. Accelerated Profile HMM Searches. *PLoS Comput Biol* **7**, e1002195, doi:10.1371/journal.pcbi.1002195 (2011).
- 74 Katoh, K. & Standley, D. M. MAFFT multiple sequence alignment software version 7: improvements in performance and usability. *Mol Biol Evol* **30**, 772-780, doi:10.1093/molbev/mst010 (2013).
- 75 Capella-Gutierrez, S., Silla-Martinez, J. M. & Gabaldon, T. trimAl: a tool for automated alignment trimming in large-scale phylogenetic analyses. *Bioinformatics* **25**, 1972-1973, doi:10.1093/bioinformatics/btp348 (2009).
- 76 Nguyen, L. T., Schmidt, H. A., von Haeseler, A. & Minh, B. Q. IQ-TREE: a fast and effective stochastic algorithm for estimating maximum-likelihood phylogenies. *Mol Biol Evol* **32**, 268-274, doi:10.1093/molbev/msu300 (2015).
- 77 Peabody, N. C. *et al.* Bursicon functions within the *Drosophila* CNS to modulate wing expansion behavior, hormone secretion, and cell death. *J Neurosci* **28**, 14379-14391, doi:10.1523/JNEUROSCI.2842-08.2008 (2008).
- 78 Geminard, C., Rulifson, E. J. & Leopold, P. Remote control of insulin secretion by fat cells in *Drosophila*. *Cell Metab* **10**, 199-207, doi:10.1016/j.cmet.2009.08.002 (2009).
- 79 Schoofs, L. *et al.* Isolation, identification, and synthesis of PDVDHFLRFamide (SchistoFLRFamide) in *Locusta migratoria* and its association with the male accessory glands, the salivary glands, the heart, and the oviduct. *Peptides* **14**, 409-421 (1993).
- 80 Koyama, L. A. J. *et al.* Bellymount enables longitudinal, intravital imaging of abdominal organs and the gut microbiota in adult *Drosophila*. *PLoS Biol* **18**, e3000567, doi:10.1371/journal.pbio.3000567 (2020).
- 81 Lopes, G. *et al.* Bonsai: an event-based framework for processing and controlling data streams. *Front Neuroinform* **9**, 7, doi:10.3389/fninf.2015.00007 (2015).
- 82 Rodriguez, A., Ehlenberger, D. B., Dickstein, D. L., Hof, P. R. & Wearne, S. L. Automated three-dimensional detection and shape classification of dendritic spines from fluorescence microscopy images. *PLoS One* **3**, e1997, doi:10.1371/journal.pone.0001997 (2008).

- 83 Sejourne, J. *et al.* Mushroom body efferent neurons responsible for aversive olfactory memory retrieval in *Drosophila*. *Nat Neurosci* **14**, 903-910, doi:10.1038/nn.2846 (2011).
- 84 Placais, P. Y. *et al.* Slow oscillations in two pairs of dopaminergic neurons gate long-term memory formation in *Drosophila*. *Nat Neurosci* **15**, 592-599, doi:10.1038/nn.3055 (2012).
- 85 Buchon, N. *et al.* Morphological and molecular characterization of adult midgut compartmentalization in *Drosophila*. *Cell Rep* **3**, 1725-1738, doi:10.1016/j.celrep.2013.04.001 (2013).
- 86 Leader, D. P., Krause, S. A., Pandit, A., Davies, S. A. & Dow, J. A. T. FlyAtlas 2: a new version of the *Drosophila melanogaster* expression atlas with RNA-Seq, miRNA-Seq and sex-specific data. *Nucleic Acids Res* **46**, D809-D815, doi:10.1093/nar/gkx976 (2018).



Figure 2

Ms neuron modulation by internal state

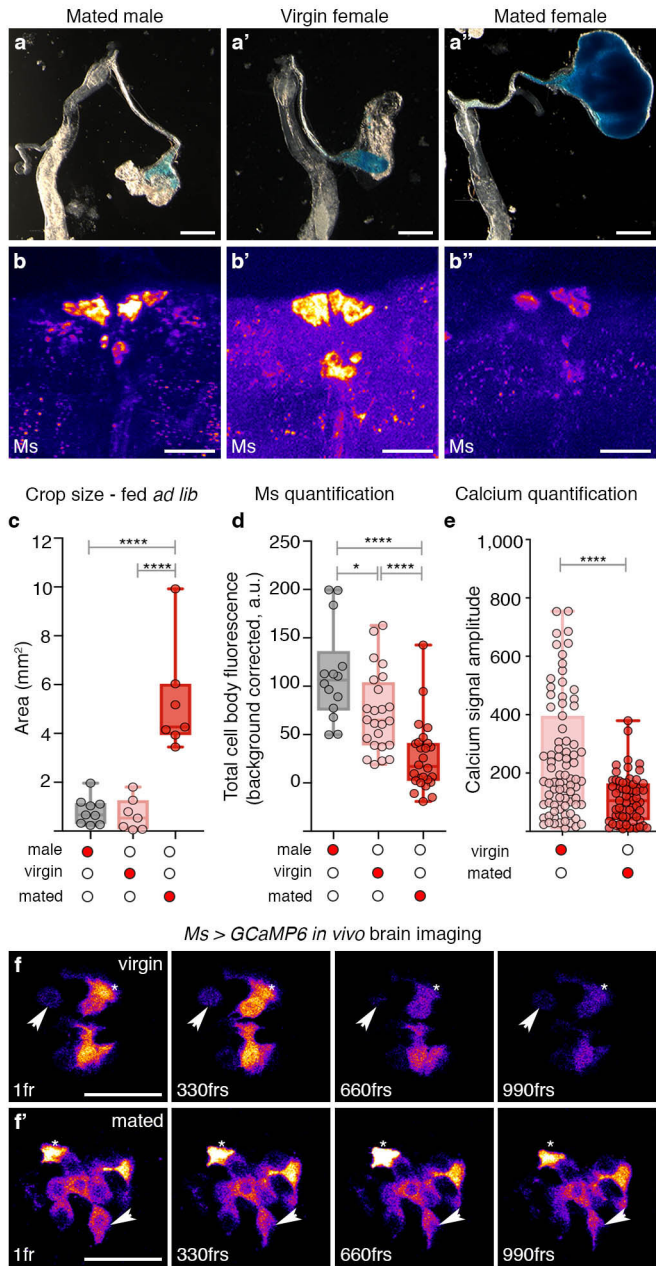
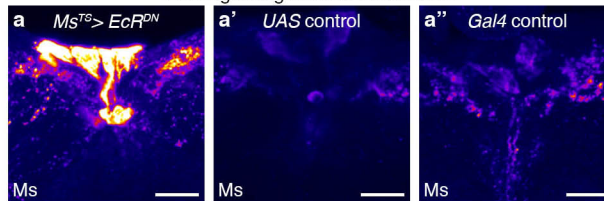


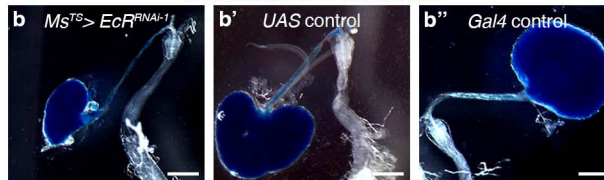
Figure 3

Ecdysone modulation of Ms neurons and crop filling

EcR signalling block in Ms neurons

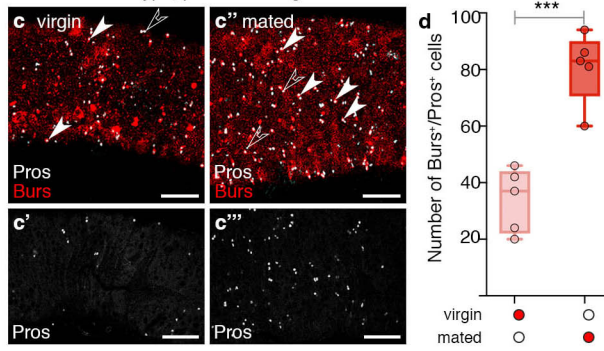


EcR knockdown in Ms neurons



Post-mating changes in Burs-positive EE cells

Wild type, posterior midgut



Burs modulation of Ms neurons and crop filling

rk knockdown in Ms neurons

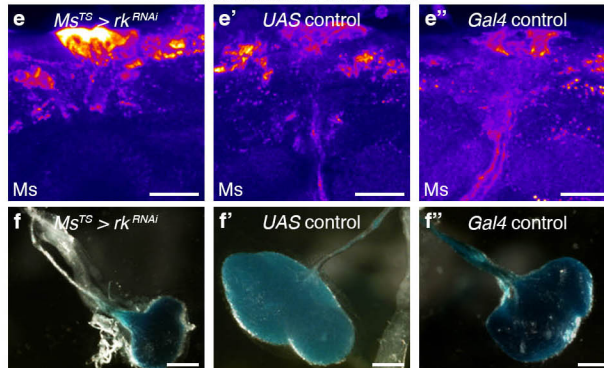
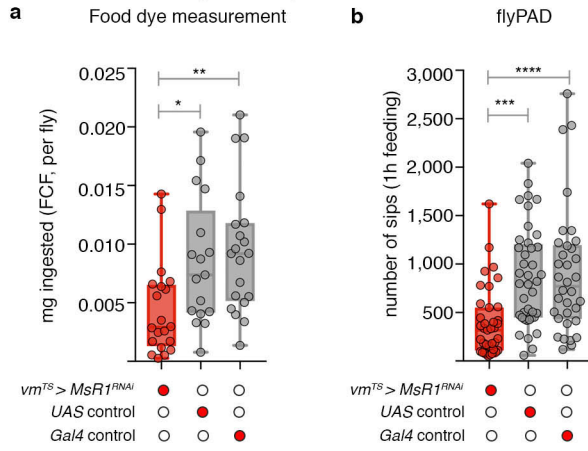


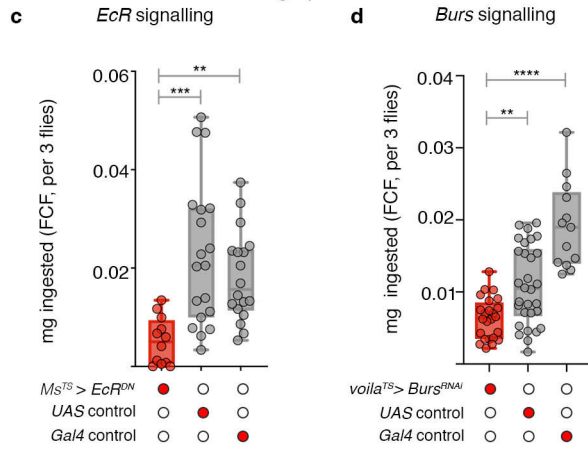
Figure 4

Crop modulation of food intake

crop muscle-specific *MsR1* knockdown

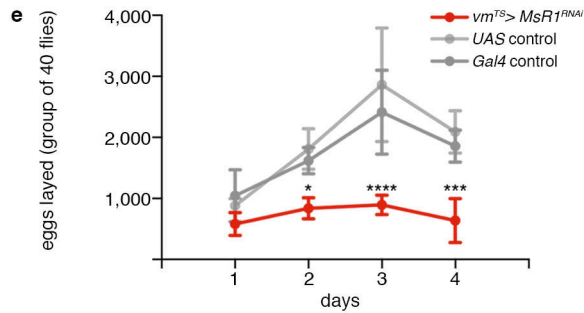


Post-mating inputs into *Ms* neurons



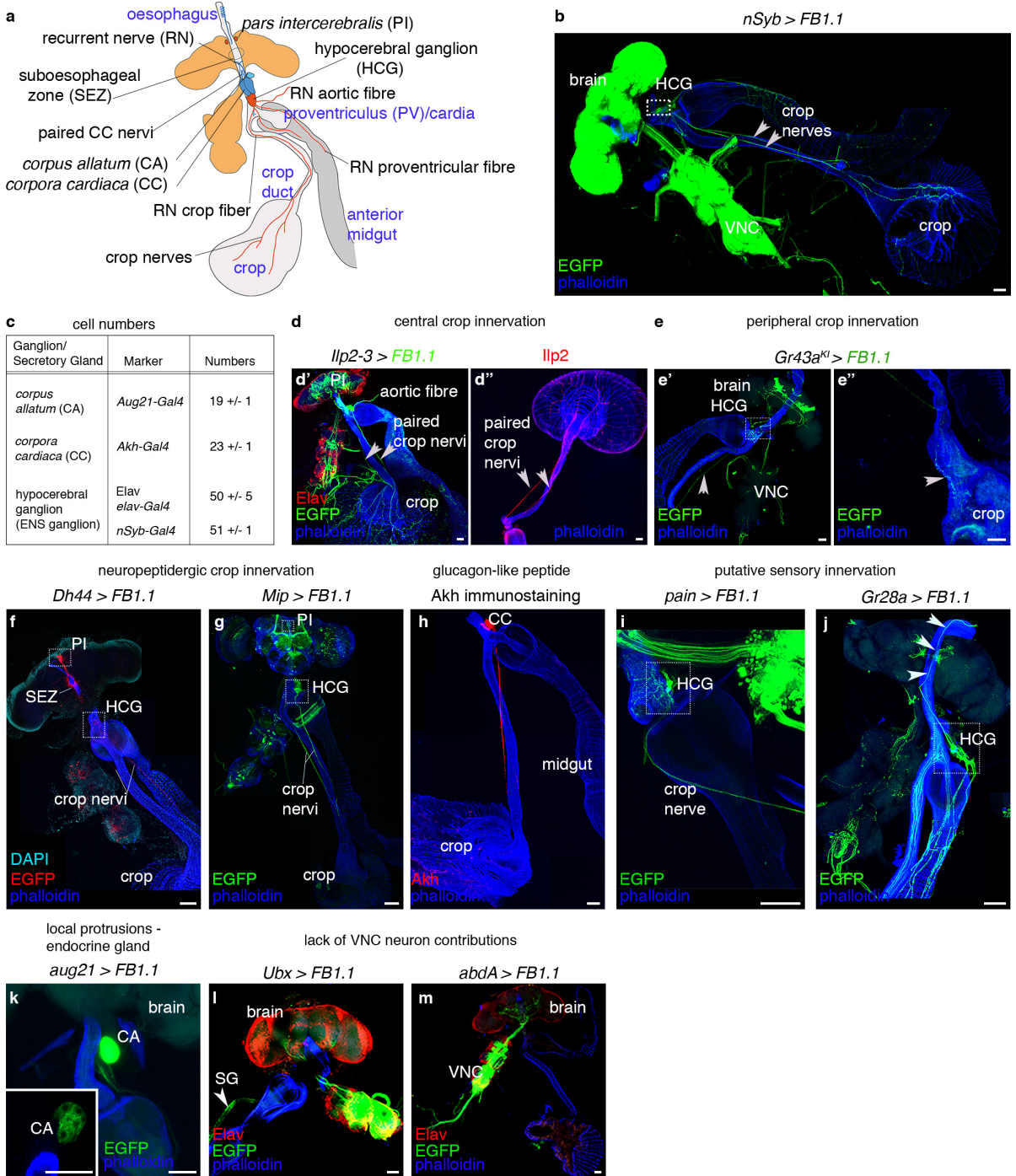
Crop modulation of fecundity

Knockdown of *MsR1* in adult crop muscles - mated females



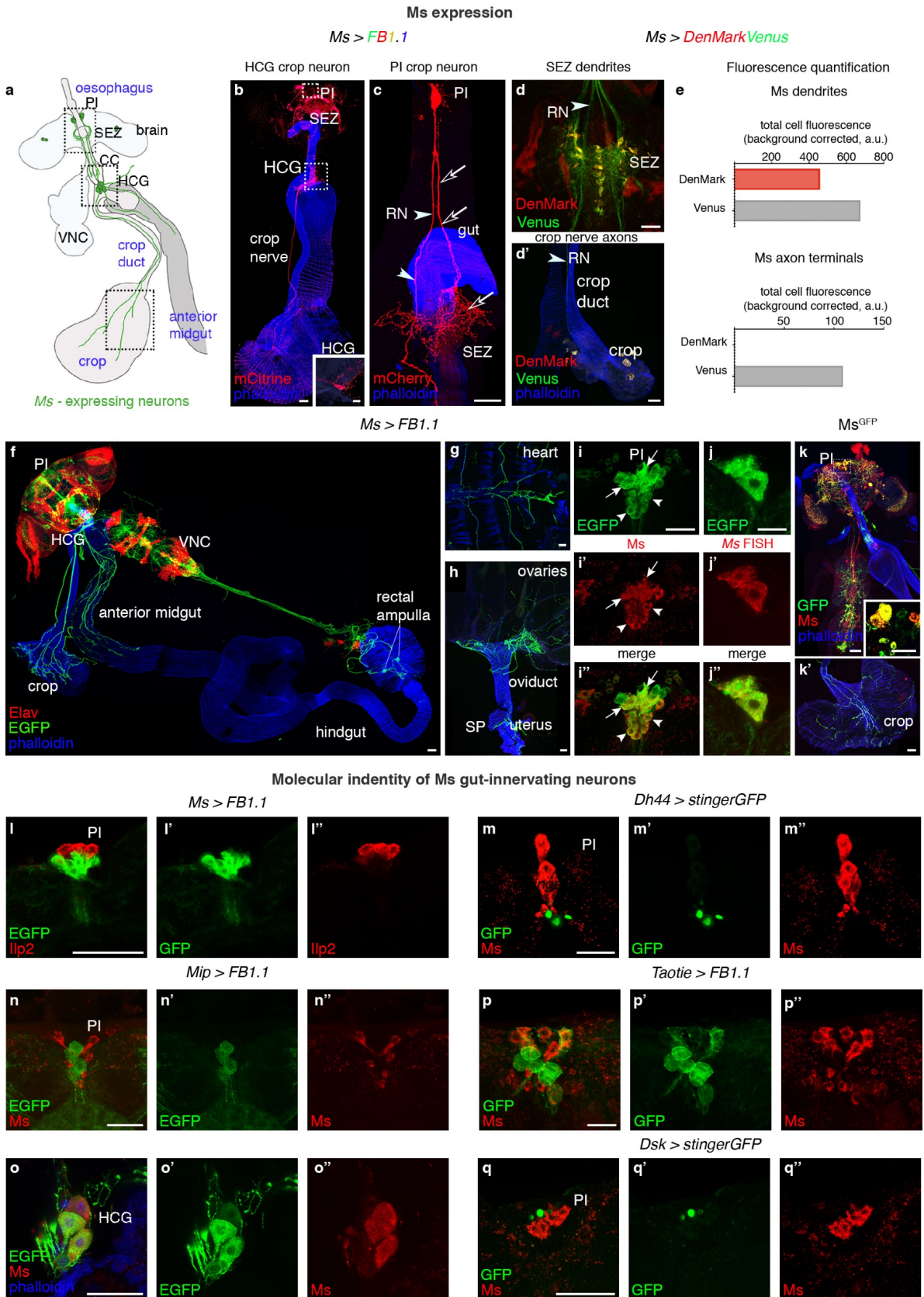
# Extended Data Fig. 1

## Crop / anterior midgut innervation : enteric neuronal subsets



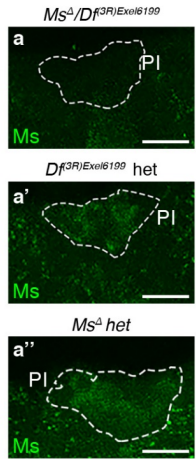


# Extended Data Fig. 3



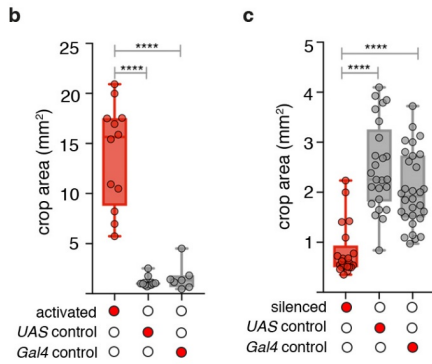
# Extended Data Fig. 4

## Ms mutant validation



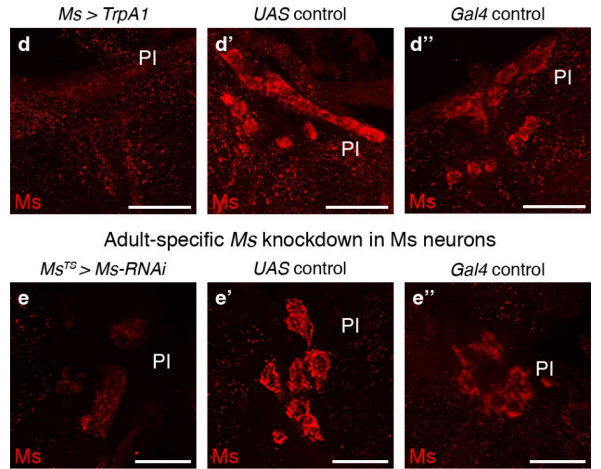
## Crop size

Ms neuron activation    Ms neuron silencing

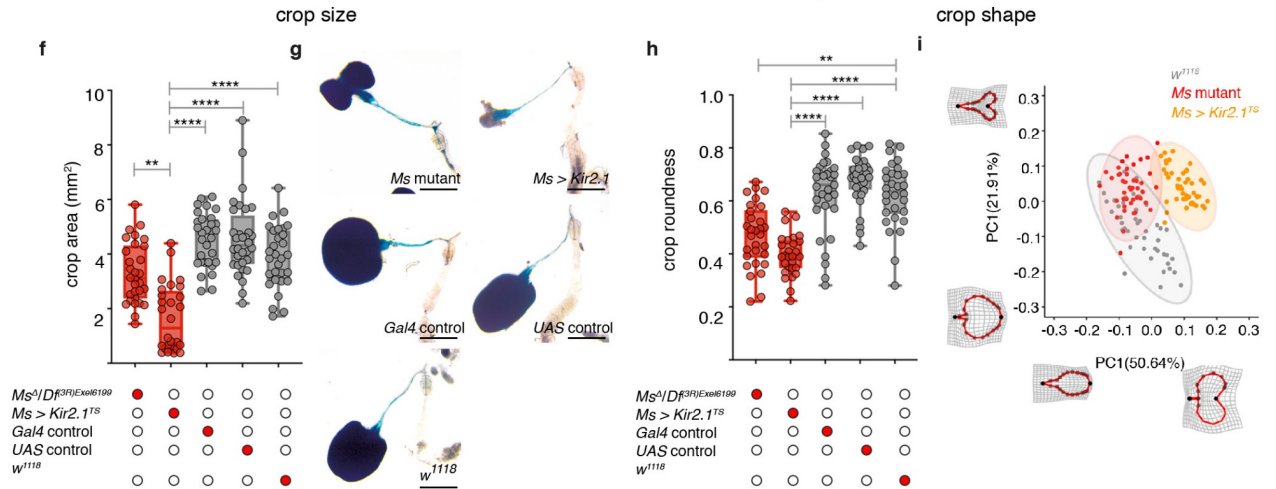


## Ms levels in PI neurons

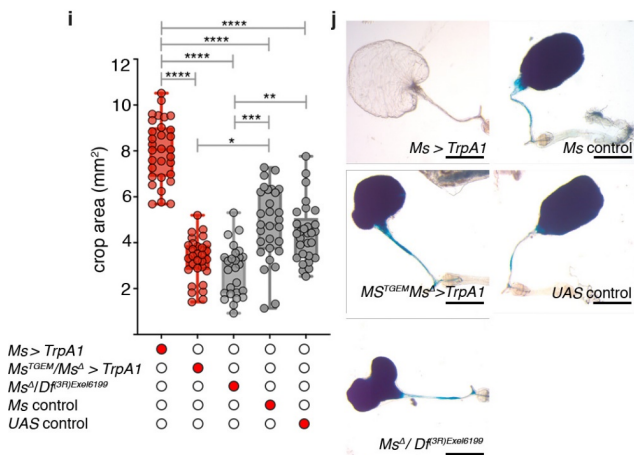
Ms neuron activation



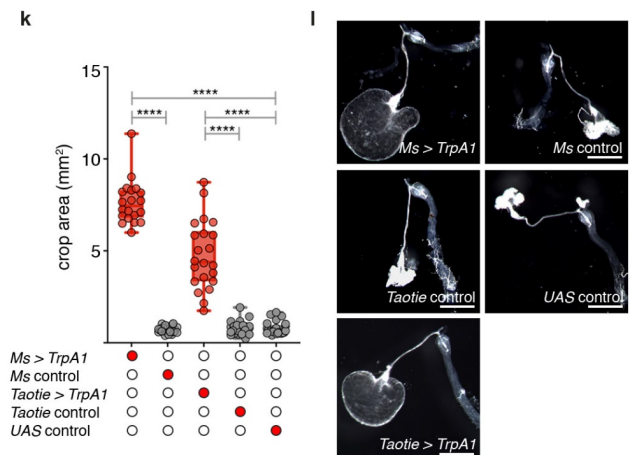
## Ms knock-out vs Ms neuron silencing



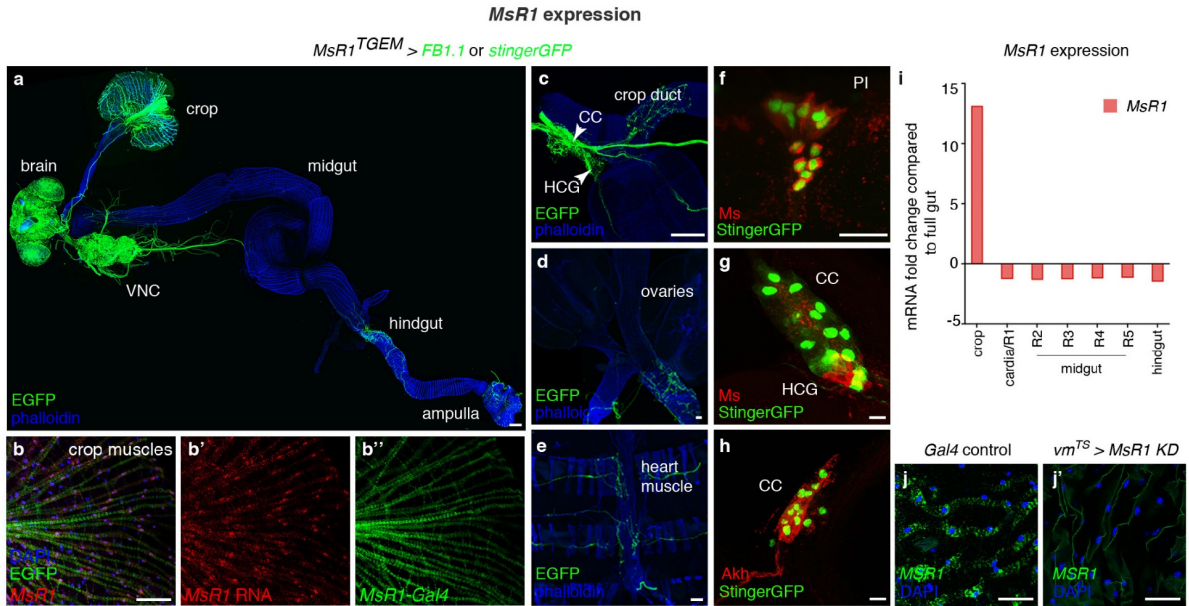
## Ms neurons activation in Ms mutant background



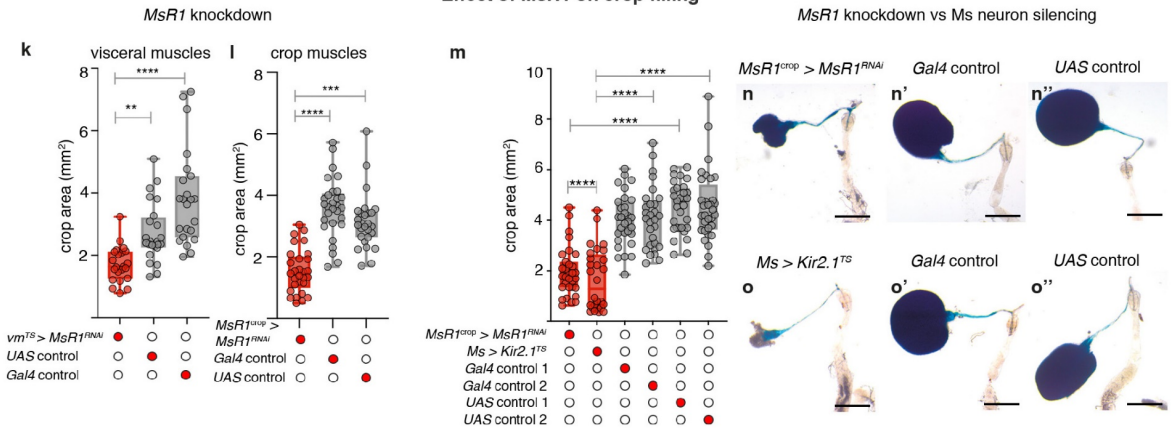
## Activation of Ms neuron subsets



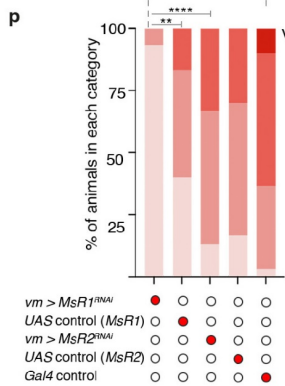
# Extended Data Fig. 5



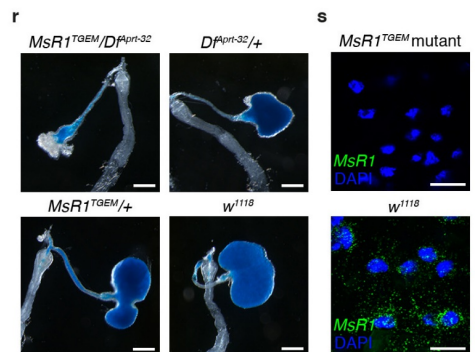
## Effect of *MsR1* on crop filling



## *MsR1* vs *MsR2* effects



## *MsR1<sup>TGEM</sup> mutant analysis*

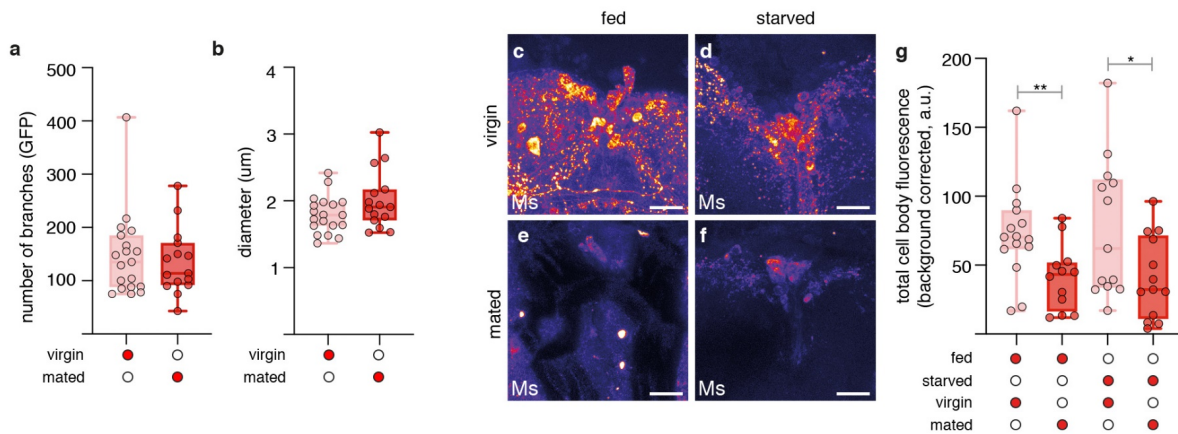


# Extended Data Fig. 6

## Modulation of Ms neurons by internal state

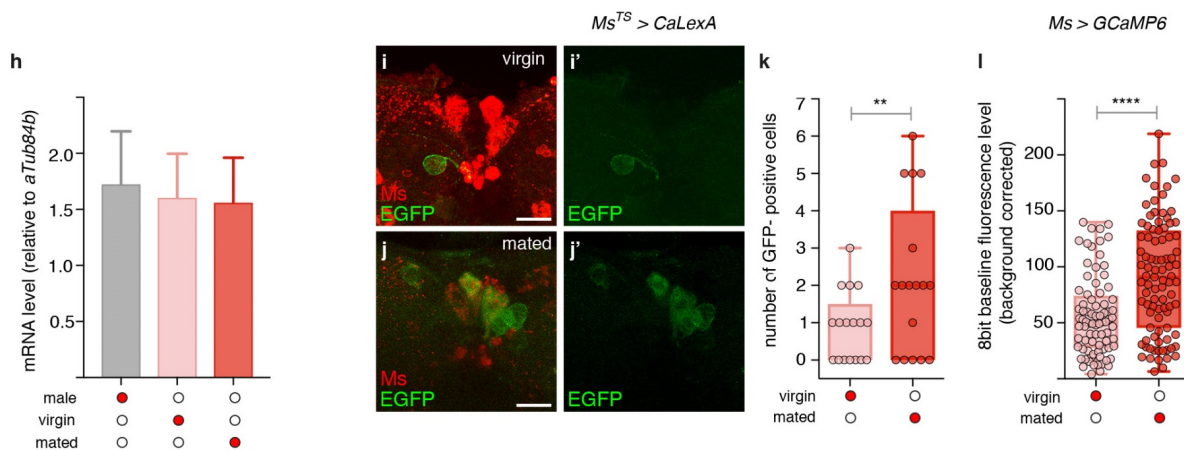
Effects of mating on Ms neuron axonal terminals

Effects of mating and starvation on Ms peptide

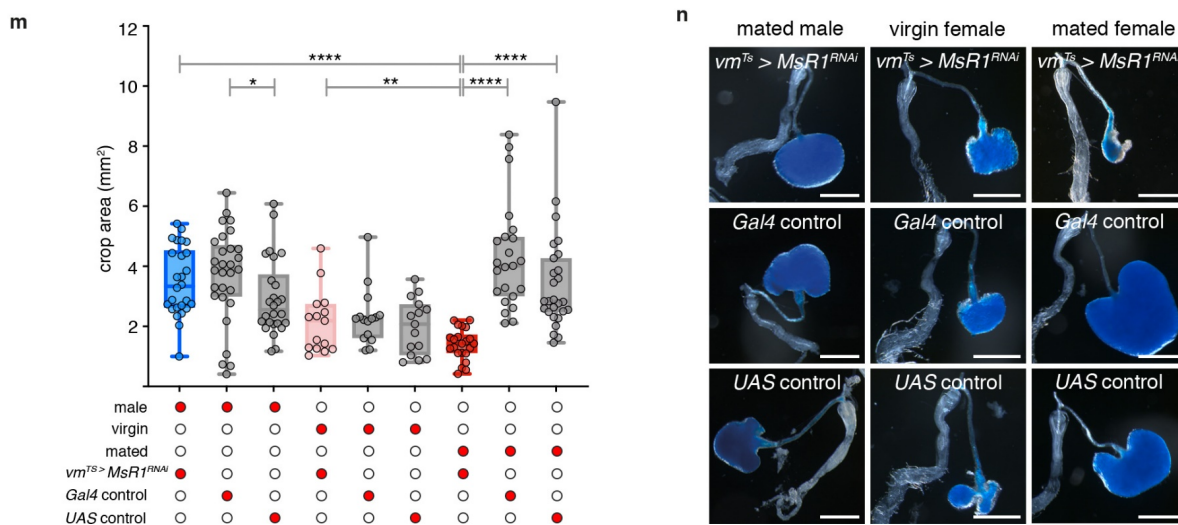


Mating-induced changes in Ms transcript

Mating-induced changes in calcium levels

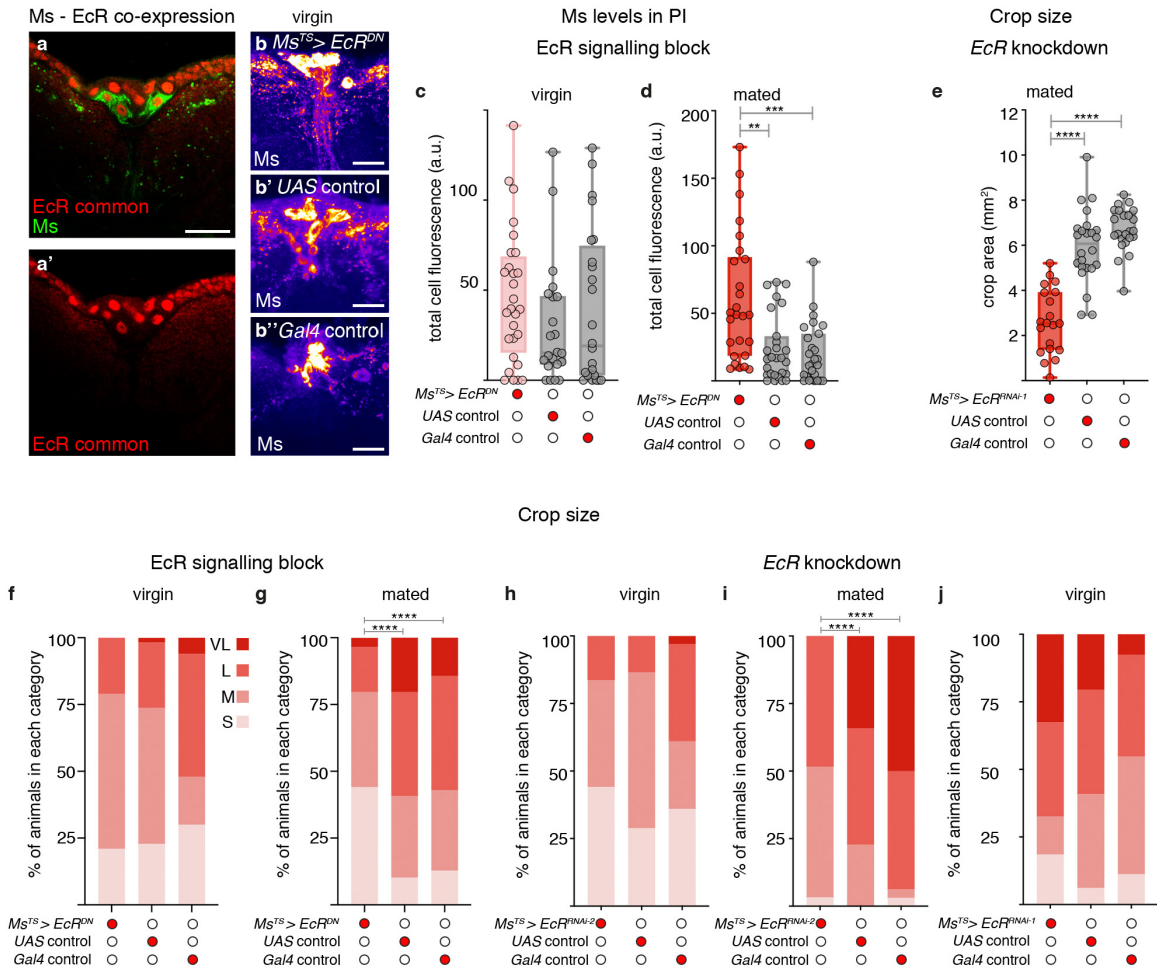


Effects of mating and sex on crop size - Ms signalling contribution



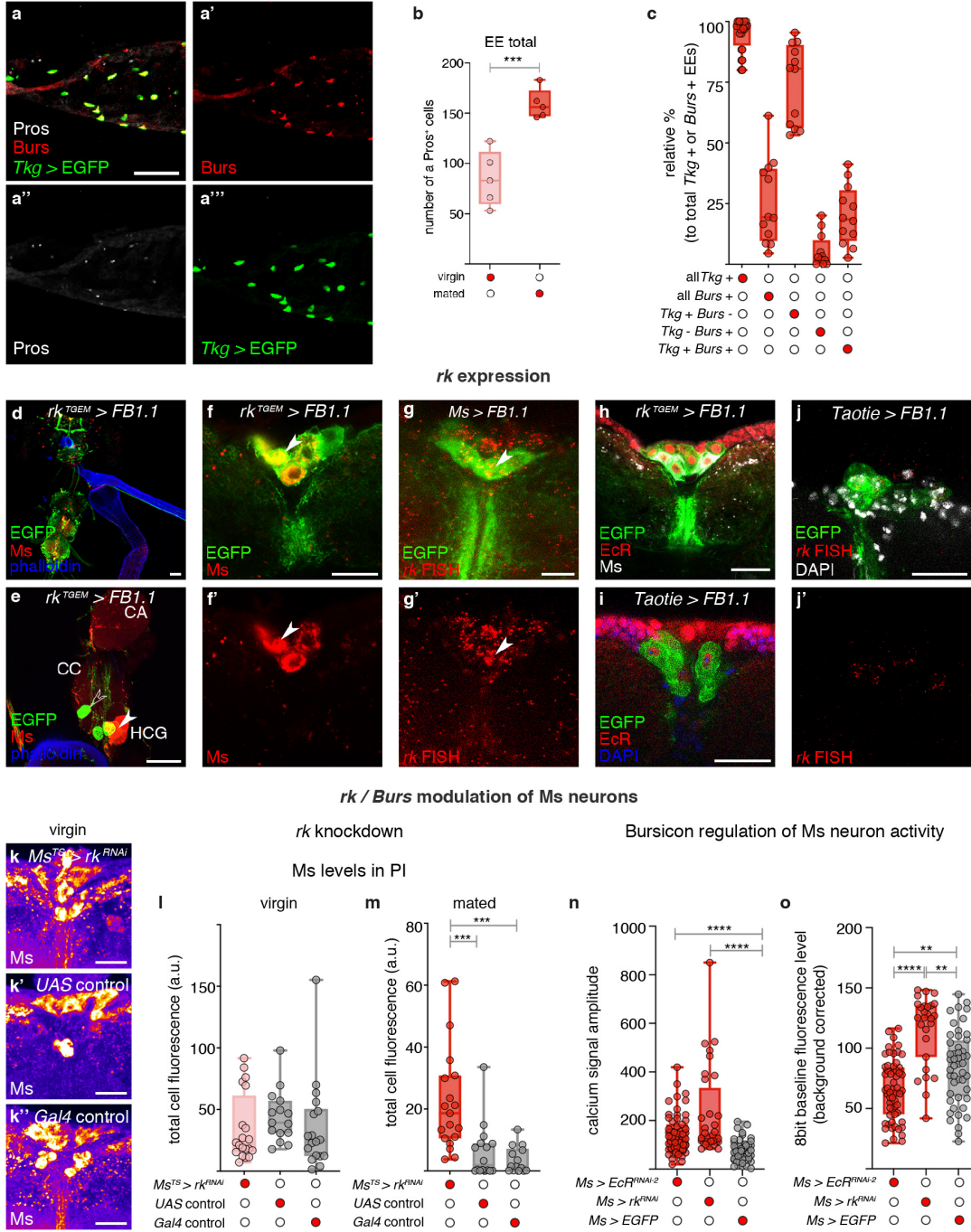
# Extended Data Fig. 7

## Ecdysone modulation of Ms neurons and crop size



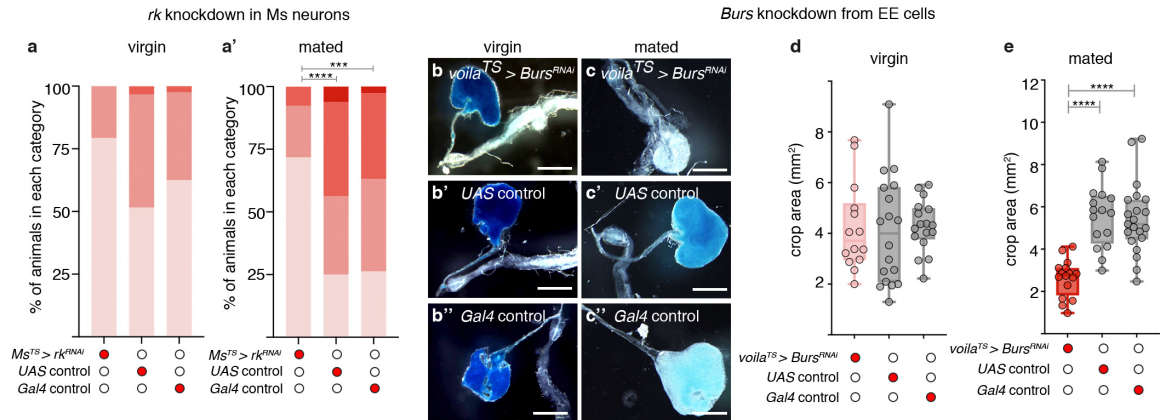
# Extended Data Fig. 8

## Regulation of Burs-positive EE cells

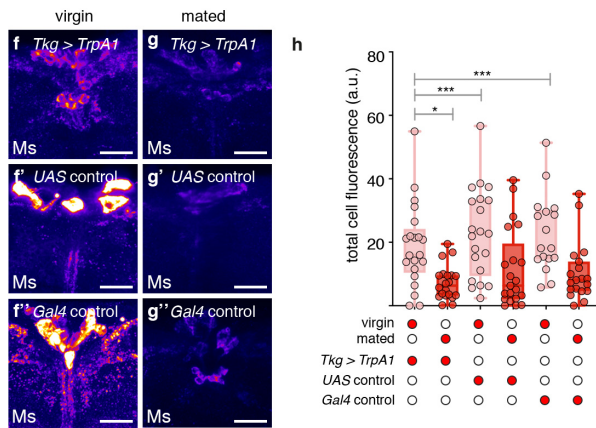


# Extended Data Fig. 9

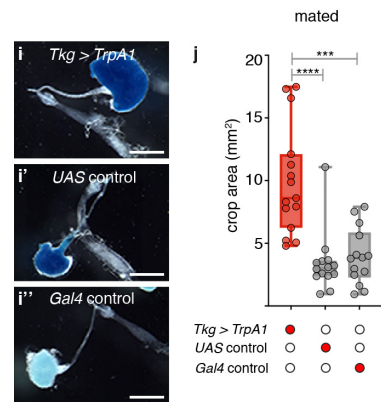
## rk / Burs modulation of crop size



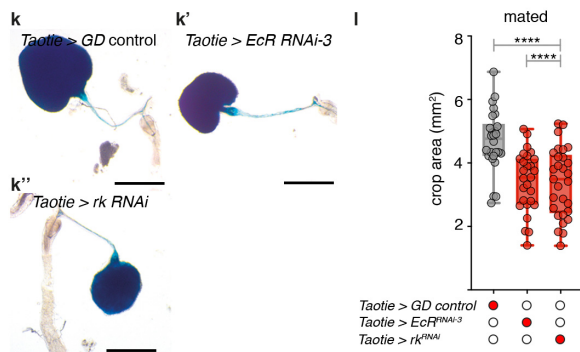
## EE control of PI Ms levels



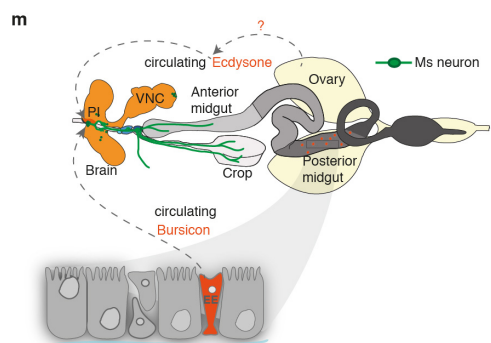
## Effect of EE cell activation on crop size



## Taotie neuron modulation of crop size via Ecdysone and Burs



## Summary



# Extended Data Fig. 10

